



Kinetic and Continuum Modeling of High-Temperature Air Relaxation

Sergey F. Gimelshein* and Ingrid J. Wysong†


Air Force Research Laboratory, Edwards Air Force Base, California 93524

Alexander J. Fangman‡ and Daniil A. Andrienko§

Texas A&M University, College Station, Texas 77840


Olga V. Kunova¶ and Elena V. Kustova**

Saint Petersburg State University, 199034, St. Petersburg, Russia

Fabio Morgado,†† Catarina Garbacz,‡‡ and Marco Fossati§§

University of Strathclyde, Glasgow, Scotland G1 1XJ, United Kingdom

and

Kyle M. Hanquist¶¶

University of Arizona, Tucson, Arizona 85721

<https://doi.org/10.2514/1.T6462>

Fully kinetic, vibrationally kinetic, and continuum solvers with varying model fidelity are used in this work to model the high-temperature relaxation of air in 7230 and 15,000 K adiabatic heat baths and a 6 km/s hypersonic flow over a cylinder. The results show significant impact of uncertainties in vibrational relaxation times and reaction rate constants on thermal and chemical relaxation, in particular, on gas temperature and species mole fractions. Most notably, these uncertainties need to be reduced for collisions that include nitric oxide. Order-of-magnitude differences in the nitric oxide dissociation and recombination rates have a large impact on the peak NO mole fraction immediately behind the shock and surface-distributed heat flux, respectively. High-fidelity kinetic and continuum approaches are found to have different reaction channels having the largest effect on species mole fractions and gas temperature: $N_2 + O$ exchange and $O_2 + O$ dissociation in the former, and $NO + O$ and $O_2 + N_2$ dissociation in the latter.

I. Introduction

DEVELOPMENT of methods and models that adequately predict fundamental physical properties and allow credible and efficient optimization for future operational high-speed vehicle systems has been a long-standing goal of research in hypersonics and space technologies. Simulation of high-altitude environments, which traditionally aims at improving flight planning designs for such systems, meets significant challenges attributed to thermal and chemical effects inherent in high-energy molecular collisions in the gas phase and at the surface. The excitation of internal degrees of freedom and dissociation of oxygen and nitrogen molecules result in a significant decrease of gas temperature inside the hot layer of gas between the

shock wave and the surface. This, in turn, affects flow observables, such as UV emissions, as well as surface properties, most notably distributed heat fluxes. Recent computational studies [1] have shown that predicted surface properties, both aerodynamic and thermal, are sensitive to the nonequilibrium thermochemistry modeling. Nonequilibrium gas flows have been the primary scope of several experimental campaigns [2–5] conducted over the last two decades. These measurements, performed to provide surface and flow properties to modelers, are an important step toward building a reference database for the validation of numerical approaches and models. Successful in many aspects, these efforts, however, fell short of providing conclusive datasets that unambiguously define the key excitation and reaction processes in high-temperature air [6]. Today, there is still a considerable level of uncertainty related not only to nonequilibrium rates and the interaction between these processes, but often even to single-temperature rates. Specific examples relevant to aerothermodynamic properties are nitrogen high-temperature dissociation and low-temperature recombination, and to flow observables, all excitation and reaction processes involving nitric oxide.

There are two primary reasons for the lack of consensus among modelers on what rates and models to use in each specific case. The first is related to the quality of underlying data that these rates are based upon. As described in Ref. [6], the main body of measurements from the 1960s and 1970s had unknown degrees of vibrational nonequilibrium, and the rates inferred from them had to rely on semi-empirical models for interpretation. There is also considerable scatter and variation among the results. Even for relatively simple cases of binary gases, experimental error bars on the order of 20% in gas macroparameters [5] often translate to much larger error bars in the excitation and reaction rates [7]. The second reason is the multi-parametric nature of nonequilibrium high-temperature air flow modeling. There are many competing processes that may influence flow observables to a different extent, and even a single process depends on many parameters. An example here is dissociation of nitrogen and oxygen molecules, which depends on internal and translational states of reacting molecules, and is further complicated by unknown energy disposal over reaction products. The complex set of processes that contribute to the measurable quantity, often supplemented by

Received 24 August 2021; revision received 19 January 2022; accepted for publication 26 January 2022; published online 21 February 2022. Copyright © 2022 by the American Institute of Aeronautics and Astronautics, Inc. All rights reserved. All requests for copying and permission to reprint should be submitted to CCC at www.copyright.com; employ the eISSN 1533-6808 to initiate your request. See also AIAA Rights and Permissions www.aiaa.org/randp.

*Aerospace Engineer, Jacobs Technology; gimel@particlematters.inc.

†Branch Chief, Combustion Devices Branch; ingrid.wysong@us.af.mil. Associate Fellow AIAA.

‡Ph.D. Candidate, Department of Aerospace Engineering, 710 Ross Street; afangman@tamu.edu.

§Assistant Professor, Department of Aerospace Engineering, 710 Ross Street; daniila@tamu.edu. Member AIAA.

¶Senior Researcher, Fluid Dynamics Department, 7/9 Universitetskaya nab.; kunova.olga@gmail.com.

**Professor, Head of Fluid Dynamics Department, 7/9 Universitetskaya nab.; e.kustova@spbu.ru.

††Ph.D. Student, Department Mechanical and Aerospace Engineering, Aerospace Centre; fabio.pereira-morgado@strath.ac.uk. Member AIAA.

‡‡Ph.D. Student, Department Mechanical and Aerospace Engineering, Aerospace Centre; ana.gomes@strath.ac.uk. Member AIAA.

§§Associate Professor, Department Mechanical and Aerospace Engineering, Aerospace Centre; marco.fossati@strath.ac.uk. Member AIAA.

¶¶Assistant Professor, Department of Aerospace and Mechanical Engineering, 1130 N. Mountain Avenue; hanquist@arizona.edu. Senior Member AIAA.

unknown level of uncertainties in the freestream conditions, is the reason that validation of specific reaction rates from heat flux or other surface measurements is often not possible. Comprehensive uncertainty quantification studies, such as Refs. [8,9], are a robust tool that is expected to help design and interpret improved experimental studies. Such studies are expected to provide an important input into what processes, and possibly flow conditions, need to be the focus of experimental research, which still needs to be the main path toward decreasing rate and model uncertainties.

Large, and sometimes unacceptable, numerical error bars that adversely affect credibility of hypersonic flow modeling have been well recognized by the research community, and remarkable progress has been made over the last few years toward improving the accuracy of numerical analysis of high-temperature nonequilibrium air flows. Both theoretical and experimental work contributed to that progress. The development of accurate potential energy surfaces for oxygen and nitrogen collisions, and the use of those surfaces in parametric quasi-classical trajectory (QCT) calculations, made available high-fidelity state-specific rates and detailed cross sections for internal energy excitation, dissociation, and exchange reactions for key collision paths [10,11]. Increasing accuracy and relevance of conditions in experimental studies, primarily those currently conducted in shock tubes, with both incident [5] and reflected [12–15] shock configurations, and in hypervelocity wind tunnel and expansion tube facilities [16,17], all promise to offer reliable data with error bars significantly lower than those of past experiments. Such theoretical and experimental achievements, as it was argued in our earlier work [18], may provide a solid basis and motivation for adopting a common set of benchmark cases in the nonequilibrium computational fluid dynamics (CFD) community, similar to the Gaseous Electronics Conference Radio Frequency (GEC RF) Reference Cell in the plasma physics community [19].

A small step in this direction was made in Ref. [18], where Hypersonic NonEquilibrium Comparison Cases (HyNECC) for nonequilibrium CFD methods were introduced (see also www.github.com/hynecc). Reference [18] presented only a tentative outline of possible flow conditions, whereas the first in-depth analysis of comparison cases was conducted in Ref. [7]. In that work, high-temperature binary-mixture oxygen and nitrogen adiabatic heat baths have been modeled with multiple two-temperature CFD, vibrational state-specific, and fully kinetic solvers. Analysis of single-temperature and nonequilibrium excitation and reaction rates has shown the largest differences for molecule–atom vibration–translation (VT) relaxation and N_2 - N_2 dissociation, especially at higher temperatures. It was noted in Ref. [7], and it is also the belief of the authors, that accurate shock-tube data on high-temperature nitrogen relaxation, preferably with error bars within 5%, may be required to address these differences. For oxygen, state-of-the-art theoretical and experiment-based relaxation rates are relatively close. Comparison of state-specific and two-temperature approaches has shown qualitative differences in the time-dependent nonequilibrium reaction rates and their ratio to the corresponding single-temperature rates. For fully kinetic and master equation (ME)-based approaches, there is a well-defined plateau observed at a time when the gas vibrational temperature approaches the translational temperature, and the thermal relaxation proceeds through a quasi steady state. There is no such plateau observed in the two-temperature solutions. Not unexpectedly, the computations also showed a major impact of the vibration–dissociation coupling on the temporal relaxation of gas properties.

In the present work, the analysis of models and methods performed in Ref. [7] for the high-temperature adiabatic relaxation of binary mixtures of oxygen and nitrogen is extended to reacting air. Such an extension, while adding more complexity due to significantly larger number of thermal and chemical processes, at the same time provides a number of opportunities. First and foremost, there is nitric oxide formed in molecule–atom exchange reactions, which is usually the easiest target for optical diagnostics, and it is thus interesting to examine factors that affect density and temperatures of this species. Second, the ongoing experimental work on reflected shocks in air [14], with their high-accuracy UV absorbance measurements that provide information on vibrational temperature and dissociation of

oxygen, provides motivation to evaluate the sensitivity of oxygen properties to various thermal and chemical processes in air. Finally, modeling air allows for replicating flight conditions, and thus one may establish a connection between thermal relaxation behind a shock wave, often approximated by adiabatic relaxation, and surface properties. To this end, both spatially homogeneous thermal bath and a flow over a cylinder are considered here. For the former, all kinetic and continuum solvers of Ref. [7] are used here, with more reaction and thermal models added for the sake of completeness, as discussed below. For the latter, the direct simulation Monte Carlo (DSMC) method and the solution of the Navier–Stokes (NS) equations are considered, with the same models as for the thermal bath.

II. Flow Conditions

There are several flow conditions considered in this work, listed here in their increasing physical and modeling complexity. The first, called hereafter Test Case 1, or TC1, is a spatially homogeneous thermal heat bath, chosen here to replicate the conditions behind a reflected shock wave in one of the experiments presented in Ref. [14]. In this case, the initial condition is a 79% N_2 -21% O_2 mixture kept at $T_{\text{trn}} = T_{\text{rot}} = 7230$ K and $T_{\text{vib}} = 300$ K, with a gas pressure of 32 Torr. The gas is then relaxed adiabatically through thermal energy transfer and chemical reactions. The conventional set of 15 dissociation–recombination and 4 exchange reactions is modeled. No ionization reactions are considered in this work, but electronic excitation is included in some cases, as discussed below. Simulations cover significantly longer relaxation time of 2 ms than 50 μ s observed in the experiment [14]. This time is sufficient to compute the peak fraction of NO species, although not long enough to reach fully equilibrium state (orders of magnitude longer times would be necessary for that, which would be prohibitively expensive for kinetic simulations).

Homogeneous bath relaxation does not take into account the thermal diffusion and gas bulk motion processes that impact gas at each spatial location in shock reflection experiments. Because of this, even though a zero-dimensional (0D) calculation may include all key collision phenomena that dominate air flows in the relevant temperature regime, the quasi-one-dimensional (quasi-1D) nature of a shock reflection in a shock tube does not allow one to use shock wave experiments for model validation. Therefore, for comparison purposes, we use here a numerical approach of Ref. [20], and apply it to calculate the shock reflection such that the aftershock conditions will approximate those of the experiment [14], as well as TC1. To accurately reproduce the conditions of the experiment, the incident shock wave velocity was set to 2.52 km/s as recorded in the experiment, and the pressure of undisturbed air was 0.07 Torr. Only the DSMC method was used in this case, as it is the only solver adjusted to conduct 1D reflected shock simulations, with gas models identical to those used in 0D modeling, as discussed in the following section. All this makes it possible to compare the experiment versus 1D DSMC results, and the latter then can be compared to 0D.

The next test case, called TC2, is also 0D adiabatic heat bath relaxation, but for significantly higher gas temperatures, with the initial $T_{\text{trn}} = T_{\text{rot}} = 15,000$ K, and $T_{\text{vib}} = 300$ K. To have noticeable impact of recombination reactions, which were practically absent in TC1, and also reasonably fast equilibration time, the initial gas pressure in TC2 is set at 20.4 atm (the corresponding number density is 10^{25} molecules/ m^3). Same as in TC1, the gas is a 79% N_2 -21% O_2 mixture. The gas relaxation is tracked for 4 μ s, the time that was found to be sufficient to reach thermal and chemical equilibrium. The main difference of the high-temperature regime of TC2 from the moderate temperature TC1 is expected to be significantly larger contribution of dissociation, both O_2 and N_2 , followed by recombination, as compared to exchange reactions dominating in TC1. Note that the temperature of 15,000 K has not yet been reached in reflected shock wave experiments so far, but it has been achieved in high-enthalpy shock tunnel experiments, such as those of Ref. [3]. In that work, a cylinder geometry was examined in High Enthalpy Shock Tunnel Göttingen (HEG) shock tunnel; the inherent feature of this geometry is that its blunt shape results in a strong shock wave

where the gas temperature reaches normal-shock values, and the aftershock relaxation along the stagnation streamline may be roughly approximated by an adiabatic heat bath.

The flow setup considered in this work replicates the experimental conditions of Run 619, given in Ref. [3]. The peak aftershock translational–rotational temperature for this test case, called TC3, was found in the earlier work [21] to be about 15,000 K; thus aftershock relaxation is expected to be relatively similar to TC2, with the exception of recombination reactions, which in TC3 occur only near the cold wall of the cylinder. In the experiment, the geometry was a cylindrical model with a radius of 45 mm and a span of 380 mm. The large aspect ratio minimizes three-dimensional (3D) effects, making the flow quasi two-dimensional (2D) at the symmetry plane, and thus a 2D configuration is modeled here. The test gas is air, and the freestream flow properties were assessed to be fully equilibrium [3], with a density of 1.547 g/m³, a temperature of 901 K, and a velocity of 5956 m/s. The freestream mass fractions were calculated as 6.5 × 10⁻⁵% N, 22.83% O, 75.431% N₂, 0.713% O₂, and 1.026% NO. The conditions correspond to a Mach and a radius-based Knudsen numbers of 8.98 and 0.00117, respectively. The cylinder temperature, set to 300 K, is assumed not to change significantly during the experimental run. Note that in the experiments [3] the cylinder surface was catalytic; therefore, to evaluate the effect of catalyticity, the present computations were conducted with and without gas–surface reactions (the former assumed a fully catalytic surface).

III. Numerical Approaches and Physical Models

Five numerical solvers are used in this work, and in some solvers, more than one gas collision model is applied to the test cases listed in the previous section. A short description of each of these is shown in Table 1, where a summary of different aspects of the collision model is presented, along with the corresponding notation used for each particular solver–model pair. The details of the solvers, approaches, and models are given in the next section.

A. DSMC Method

The DSMC method [40] is used as the fully kinetic approach. It is applied here to model the spatially uniform adiabatic heat bath relaxation cases, a 1D reflected shock wave, and 2D cylinder flow. All DSMC simulations shown in this work are performed with the SMILE [22] code. The variable hard sphere model [41] is applied with interaction parameters listed in Table II of Ref. [21], calculated from the viscosity–temperature data of Ref. [42]. The internal energy modes are discrete, both rotational and vibrational. Morse anharmonic oscillator model is used to calculate the vibrational energy

levels of molecular species O₂, N₂, and NO, with the corresponding number of levels 47, 59, and 49. Note that these numbers differ slightly from those used in the other two vibrational state-specific approaches due to small differences in the assumed anharmonicity of the oscillator, but a separate sensitivity study conducted in DSMC suggests such differences have little impact on results. The Larsen–Borgnakke (LB) model [43] for discrete energy levels [44] is used to compute the rotation–translation energy transfer. The excitation of the electronic degrees of freedom is taken into account through energy transfer between electronic and translational modes modeled with the approach proposed in Ref. [45].

Different gas models are applied to compute internal energy transfer between vibrational and translational modes, as well as chemical reactions. In the first model, DSMC-M1, used as the baseline in our previous work [7], the state-to-state (STS) 3D Forced Harmonic Oscillator–Free Rotator (FHO-FR) [23] model is used for VT energy transfer in molecule–molecule collisions, with the DSMC implementation discussed elsewhere [46]. The discrete LB model [47] is used to simulate the VT energy exchange in molecule–atom collisions, with temperature-dependent vibrational collision numbers based on QCT calculations [48], along with a DSMC correction [49]. Vibration–vibration (VV) energy transfer is modeled with the empirical near-resonant approach [50]. The extended Bias model [51,52] is used for dissociation and recombination [53] reactions, with parameters given in Ref. [53]. The total collision energy (TCE) model [41] is used for the exchange reactions. The only difference of model DSMC-M2 from DSMC-M1 is that VV exchange is turned off in the former.

In DSMC-M3, the VT energy transfer for molecule–molecule collisions is performed with the LB method using the vibrational collision numbers based on the semi-empirical Millikan–White correlation [34] with Park’s high-temperature correction [54]; the VV transfer was not taken into account. The TCE model [41] is used for all reactions, with reaction rates at equilibrium reproducing those of the Bias model [21]. The reaction rate constants used in this work are summarized in Table 2 of [21]. Model DSMC-M4 differs from DSMC-M3 only by the reaction rate constants: in DSMC-M4, those are taken from Park’s recommendations [55]. In all four DSMC models, the Gibbs free energy approach is used to set the reverse reaction rate constants, with thermodynamic properties tabulated in Ref. [56]. For gas–surface collisions, the Maxwell model with full energy and momentum accommodation is used. A fully catalytic wall is modeled with the approach detailed in Ref. [21].

B. Master Equation Model

The ME model is a high-fidelity thermochemistry model that combines the accuracy of the kinetic simulations and the efficiency

Table 1 Summary of models

Solver	Approach	VVT model	Chemistry model	Chemical rates	Detailed balance	Notation
SMILE [22]	DSMC	LB, 3D FHO-FR [23], VV	Bias, TCE	SMILE	Gibbs	DSMC-M1
		LB, 3D FHO-FR [23]	Bias, TCE	SMILE	Gibbs	DSMC-M2
		LB	TCE	SMILE	Gibbs	DSMC-M3
		LB	TCE	Park	Gibbs	DSMC-M4
ME [24]	ME	State-resolved QCT [25–28]	State-resolved QCT [25–28]	QCT based	Partition function based	ME
STS [29]	Continuum	State-resolved FHO [30] with corrections [31] for VT exchanges	State-resolved based on modified Marrone–Treanor model fitted to QCT [32]	[32]	Partition function based	STS
SU2-NEMO [33]	Navier–Stokes	2T Millikan–White–Park [34,35]	Park [36], preferential	[35,37]	Gibbs	SU2-NEMO, Gibbs-P
			2T Park [36], nonpreferential	[35,37]	Gibbs	SU2-NEMO, Gibbs-NP
LeMANS [38]	Navier–Stokes	2T Millikan–White–Park [34,35]	Park[36], preferential	[35,37]	Gibbs	SU2-NEMO, Gibbs-P
			2T Park [36], nonpreferential	[35,37]	Gibbs	LeMANS, Gibbs-NP
			2T Park [36], MMT [39], preferential	[35,37,39]	Gibbs	LeMANS, MMT

of the continuum approach. Kinetic data in the ME approach are obtained via the QCT method. A system of MEs, similar to that of the STS model in the following section, allows for fast integration of governing equations in time with variable time-stepping and error control. Potential energy surfaces employed in the present work are of the highest accuracy currently available in the open literature.

QCT trajectories are initialized with rotational states sampled according to Boltzmann statistics. The initial vibrational state of the target species is fixed for each trajectory batch and runs from the ground to the final state before the dissociation limit. The O_2 , N_2 , and NO energy ladders contain 44, 60, and 48 vibrational states, respectively. Collision energies between target species (O_2 , N_2 , or NO) and projectile species (O, N, O_2 , or N_2) range between 0.05 and 10 eV. QCT simulation of the O_2 -O system includes all nine potentially energy surfaces (PES) that correlate with the O_3 ground electronic state [26]. N_2 -N kinetic data are taken from the database by Jaffe et al. [27] and interpolated on the present vibrational ladder. O_2 - O_2 and N_2 - N_2 rate coefficients are obtained on the triplet O_4 PES [25] and singlet N_4 PES [28]. The Zeldovich exchange mechanisms are included as discussed in [57,58]. Collisions of NO with other molecules (O_2 , N_2 , and NO) are neglected, as high-fidelity QCT data are currently unavailable for these interactions. To avoid modeling low-probability events, i.e., collisions between two molecules in excited vibrational states, the initial vibrational state of molecular projectiles is given by the ground and first vibrational states only.

Overall, the kinetic database comprises approximately 10 billion trajectories across 10 translational-rotational temperatures between 2000 and 20,000 K. The database includes rate coefficients of inelastic, exchange, swap-dissociation, double-swap, direct dissociation, and double dissociation channels [59]. The original rate coefficients are resolved with respect to the initial and final vibrational states of the molecular reactants and products; however, the database is reduced to reflect specifics of energy exchange at hypersonic temperatures. Under present conditions, VV energy transfer in pure gases is of minor importance, and bound-bound transitions are primarily governed by the VT energy exchange. For this reason, VV energy transfer is neglected, and the bound-bound rate coefficients are reduced to the form $K_{v \rightarrow v'}$, where v and v' are the initial and final vibrational states, respectively.

The system of MEs—describing the temporal evolution of the number densities of vibrational states and atomic species—comprises a set of coupled ordinary differential equations (ODEs), which are integrated from an initial thermal nonequilibrium state. A single simulation of an adiabatic relaxation case takes 2 core-min.

C. State-to-State Approach

The STS approach is designed to describe fully coupled non-equilibrium vibrational and chemical kinetics and transport properties of reacting gas mixtures in the frame of the continuum approach. The mathematical model of the approach is based on the generalized Chapman-Enskog method [60] and includes equations for the vibrational level populations of molecules and the number densities of atoms coupled to the fluid dynamic equations. Compared to the ME approach, it uses simplified models for the reaction rate coefficients but, in the general case, the STS approach can be applied to both inviscid and viscous gas flow simulations because it includes the constitutive relations for state-resolved transport terms and algorithms for the STS transport coefficients evaluation [61,62]. In the present study, it is applied for modeling spatially homogeneous adiabatic heat bath relaxation, and therefore transport processes are not taken into account. A detailed description of the STS model for inviscid air mixture flows is given in [29].

The vibrational energy ladder is described by an anharmonic oscillator and includes 68/47/53 states for $N_2/O_2/NO$ molecules, respectively. The electronic excitation of species is neglected, and we assume that they remain in the ground electronic state. The kinetic scheme includes state-resolved chemical reactions (dissociation and recombination reactions, chemical exchange reactions $N_2 + O \rightleftharpoons NO + N$ and $O_2 + N \rightleftharpoons NO + O$), one-quantum VT energy transfer, and VV energy exchanges in the N_2 - N_2 , O_2 - O_2 , and N_2 - O_2

interactions. The state-resolved rate coefficients of vibrational energy exchanges are calculated using the FHO model [30] with corrections of steric factors for VT transitions obtained in [31] by fitting vibrational relaxation times to existing experimental and numerical data. Rate coefficients of chemical reactions are calculated using the Marrone-Treanor and Aliat models [63,64] generalized in [65,66] in order to take into account temperature dependence of the model parameters and the effect of vibrational excitation of the reaction product. The latest set of parameters for state-resolved chemical reactions in air is proposed in [32] on the basis of recent QCT data. The detailed balance principle is used for calculation of the rate coefficients of backward processes.

The resulting system of ODEs was integrated numerically using the MATLAB package and its *ode15s* function (a variable-step, variable-order [from 1 to 5] solver) designed for solution of stiff ODEs.

D. CFD Approaches: 2T Model

CFD approaches are also used to model the 0D adiabatic heat bath relaxation and the hypersonic flow over a cylinder. The two codes used are the open-source SU2-NEMO [33] (NonEquilibrium Models) code and LeMANS code [38,67]. Thermochemistry models are implemented into SU2-NEMO via linking to the Mutation++ library [68] (Multicomponent Thermodynamic and Transport Properties for Ionized gases in C++), which provides algorithms for the computation of thermodynamic and chemical kinetic gas properties. LeMANS was developed as a CFD code with a focus on thermochemical nonequilibrium capabilities. The two codes are included here to provide a comparison between different solvers with intricate implementations that are expected to provide similar results. The 0D test case is modeled by using a 5×5 two-dimensional grid with a symmetry boundary condition applied to all boundaries for both LeMANS and SU2-NEMO. The flow over a cylinder is modeled by using a 200×200 two-dimensional grid with a symmetry boundary condition applied to the stagnation line for LeMANS. Cells were clustered near the surface with a cell height of $0.1 \mu\text{m}$ near the surface and a grid convergence study was completed. SU2-NEMO used a different grid, with 200 cells along an half-cylinder surface and 340 elements from the body to the inflow boundary, from which the nearest cell to the body presented an height of 0.8 nm. Similar to LeMANS, a grid convergence study was conducted. The mesh used for SU2-NEMO was also simulated using LeMANS, which resulted in a less than 1% difference in convective heating along the surface compared to the original mesh LeMANS used.

In terms of numerical approaches, SU2-NEMO uses a finite-volume edge-based formulation with the AUSM scheme [69], whereas LeMANS uses the finite-volume method with a modified Steger-Warming Flux Vector Splitting scheme [70]. SU2-NEMO uses a second-order backward-difference discretization to address time evolution, whereas LeMANS uses an explicit first-order accurate time integration for these cases.

The physical models used in each of the CFD codes are similar. The two-temperature model by Park [36] is used, where the translational energy mode is assumed to be at equilibrium with the rotational one, and the vibrational energy mode is assumed to be at equilibrium with the electronic one. This assumes that the rotational and translational energy modes of all species can be described by a single temperature T_{tr} because the rotational energy equilibrates with the translational energy in just a few collisions. Furthermore, this assumes that the vibrational and electronic energy modes of all species and the electron translational energy mode can be described by another single temperature T_{ve} . The internal mode energies are defined on the basis of the Rigid-Rotor/Harmonic Oscillator model (RRHO). The change in the vibrational energy of the mixture is accounted for as the sum of the VT energy transfer and energy exchanges due to chemical activity. The rate of energy exchange between the translational and vibrational energy modes follows the Landau-Teller model [71] with the Millikan and White [34] coefficients together with the Park correction [35] for the calculation of relaxation times. The forward reaction rates are defined according to the modified Arrhenius equation, with the controlling temperature

determined by Park’s two-temperature model [36]. The dissociation reactions are controlled by a combination of the translational–rotational and the vibrational–electron–electronic temperatures ($T_c = T_u^a T_{ve}^b$) to account for the fact that vibrationally excited molecules are more likely to dissociate. This work sets the values of a and b to 0.5. The forward reaction rates are calculated using the Arrhenius curve fits with the controlling temperature, where the reaction rate coefficients are taken from [35,37]. The backward reaction rates are obtained from the equilibrium constants, as detailed in Refs. [55,72]. The change in vibrational–electronic energy of the mixture due to the production/destruction of species follows two different models: non-preferential and preferential dissociation models [73]. The former model assumes that molecules dissociate/recombine at the average vibrational energy of the cell, at the given vibrational temperature, whereas the latter accounts for the fact that molecules only dissociate/recombine at higher vibrational levels.

In this work, a simple preferential model is used, where the value of energy added or removed is 30% of the dissociation energy. The backward reaction rates are determined from the equilibrium constants, which are calculated as a function of the Gibbs free energy [73]. The primary difference in physical models between the two codes is how each handles electronic energies. In both codes, the species electronic energy $e_{el,s}$ is modeled by

$$e_{el,s} = \begin{cases} \frac{R_u \sum_{i=1}^{\infty} g_{i,s} \theta_{el,i,s} \exp(-\theta_{el,i,s}/T_{ve})}{M_s \sum_{i=1}^{\infty} g_{i,s} \exp(-\theta_{el,i,s}/T_{ve})} & \text{for molecules and atoms,} \\ 0 & \text{for electrons} \end{cases} \quad (1)$$

where $\theta_{el,i,s}$ and $g_{i,s}$ are the characteristic electronic temperature and the degeneracy of the i th energy level, respectively. This model is used because it is accurate for the low electronic energy levels, and the energy contribution of the higher levels, where the model loses accuracy, is negligible [74]. The LeMANS code takes the necessary data from Ref. [38], whereas SU2-NEMO, through Mutation++, and uses the spectroscopic data from the Gurvich tables [75,76]. Mutation++ uses a pragmatic approach for truncating the partition function by matching the species data of Gurvich using electronic specific data for vibration. In addition to Park’s two-temperature model, LeMANS also uses the Modified Marrone–Treator (MMT) chemical kinetics model, which is a recently constructed two-temperature model developed from ab initio quantum chemistry data [39,77]. The MMT model is based on the Marrone–Treator preferential dissociation model [78] with a modification to account for the effect of rotational energy.

IV. Vibrational Energy Transfer Rates

A. Molecule–Atom Collisions

Nonequilibrium high-temperature air flow modeling to a large extent depends on what thermal and chemical rates are imposed, explicitly by direct input or implicitly through models and assumptions. The most straightforward approach for evaluating the importance of rates used in different models, and for assessing their potential impact in simulations, is to compare them at thermal and chemical equilibrium conditions in the temperature range of interest. In the most general case, this should refer to all collision-related processes that contribute to high-temperature air relaxation, starting from transport properties, i.e., viscosity, diffusion, and thermal conduction, to energy transfer between translational, rotational, and vibrational modes, to electronic excitation, and finally, to chemical reactions. The latter refers to binary reactions of dissociation and exchange, three-body collisional recombination, and various ionization processes. However, many of these processes are of a lesser importance, whereas some others are fairly well known, and thus with a large number of energy transfer and reactive channels of a five-species air, one needs to limit the scope of such comparison to only processes that are relevant for each particular case. The primary focus of this work is the UV observables O_2 and NO. Therefore, here we consider the key collision processes that are expected to affect the

flow, and impact the vibrational populations of these species. Note that the vibrational excitation and dissociation of oxygen in collisions with O and O_2 were examined in detail in the previous work [7], and only a short summary is given here. The VT relaxation for both O_2 – O_2 and O_2 –O collisions was found to be noticeably slower in the state-specific approaches than in the fully continuum ones (the VT relaxation in the former is based on QCT and 3D-FHO results, whereas the latter use the semi-empirical Millikan–White correlation with Park’s correction). The single-temperature rate constants for molecular oxygen dissociation, used in different approaches, are relatively close, within approximately a factor of two for higher, and 50% for lower temperatures. For N_2 – N_2 collisions, the vibrational relaxation is slower at higher temperatures for state-specific collisions, whereas the dissociation rates differ significantly only at temperatures about 10,000 K.

Oxygen dissociation is a relatively fast process that typically proceeds quickly in the hot region behind a high-Mach-number shock wave. Newly created oxygen atoms then excite the vibrational mode of nitrogen, thus significantly accelerating its dissociation. The N_2 –O collisions may therefore be important and need to be accurately modeled. The corresponding vibrational relaxation times for this interaction, used in different numerical solvers, are presented in Fig. 1a. Both NS codes apply the conventional Millikan–White–Park correlation with $p\tau_v \propto T^{1/3}$ dependence, and the coefficients in the expression taken as recommended in Ref. [79]. SU2-NEMO and LeMANS $p\tau_v$ is denoted “NS.” The relaxation time used in the DSMC code is based on the experimental data of [80], with significantly weaker temperature dependence, and slower relaxation at higher temperatures. The ME approach is based on the recent QCT calculations, and the resulting $p\tau_v(T)$ dependence is the strongest of all solvers considered here. Interestingly, the relaxation time of ME- and NS-based approaches is very close at $T > 8000$ K. The STS solver uses the FHO-based relaxation rates, and its relaxation rate is close to that of the NS solvers at low temperatures, but much slower at high temperatures.

The above comparison shows that there are significant differences in the vibrational relaxation rates used in the five numerical solvers considered here. Clearly, the choice of the relaxation rate or, for state-specific methods, of the parameters of the model that defines it should depend on the available theoretical and experimental data specific to that particular collision type. At this time, though, there are few collisions where there would be a consensus among modelers on what particular rate must be used. One example where this would be the case is the vibrational relaxation in collisions of oxygen and nitrogen molecules, where the Millikan–White correlation was traditionally considered very reliable for temperatures below 8000 K. However, recent high-accuracy measurements [12] indicate that even that seemingly reliable correlation may have larger-than-expected error bars, as the measured VT relaxation in O_2 collisions was found to be on average a factor of 2 slower than that of Millikan–White. The situation is even more complex for other collision types, where there is little or no experimental data, and theoretical predictions, such as QCT and quantum mechanics based, often differ by over an order of magnitude. Therefore, it may be hard or impossible at this time to evaluate the actual accuracy of relaxation or reaction rates for such collisions, even when the difference is as significant as in Fig. 1a.

The uncertainty in the vibrational relaxation time for NO–O collisions appears to be at least as big as for N_2 –O, which is illustrated in Fig. 1b. The DSMC solver uses the expression of Ref. [48] extended to NO–O collisions, where the relaxation time depends weakly on temperature, and $p\tau_v$ somewhat increases with T . The slope is very similar in the ME approach, for which the relaxation rate follows QCT calculations, although the magnitude is approximately two times lower than that in DSMC. The STS relaxation rate is close to ME at moderate temperatures, but becomes significantly slower as the temperature increases. Summarizing, qualitative differences in N_2 –O VT relaxation rates assumed or applied in different solvers may be an indication that better theoretical and, ideally, accurate experimental data may be necessary to provide some guidance on that relaxation. This is especially relevant for higher temperatures, when most oxygen molecules have already dissociated, reducing the

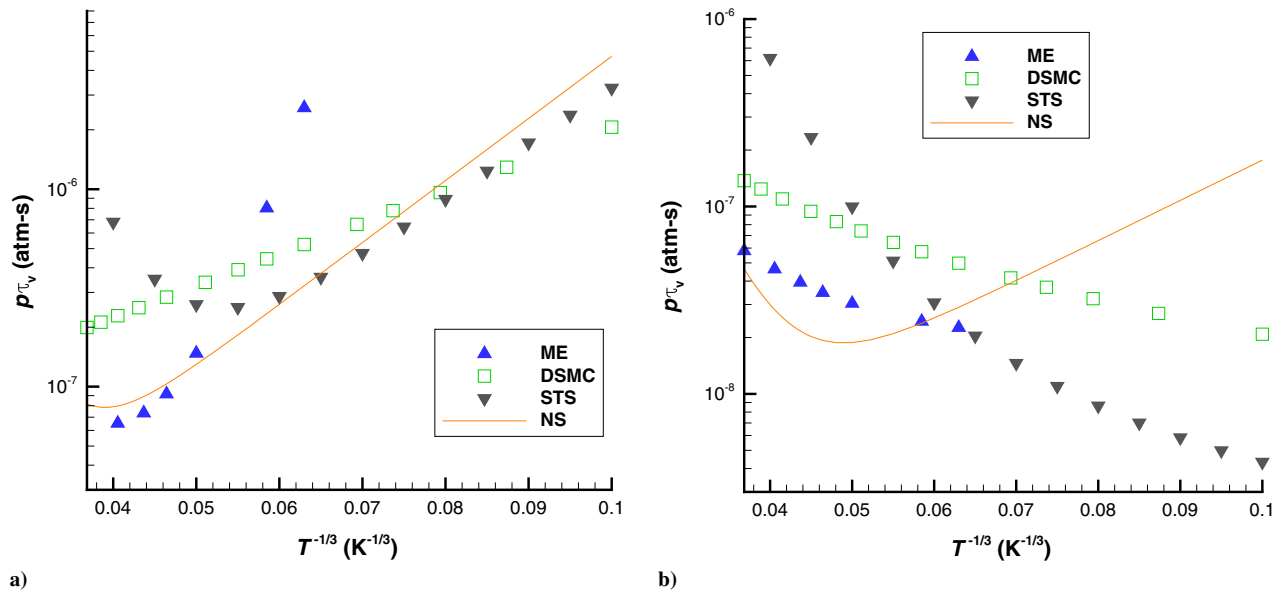


Fig. 1 Vibrational relaxation time for N_2 -O (a) and NO -O (b) collisions.

impact of the VV energy transfer in O_2 - N_2 collisions, and making collisions between N_2 and O the primary source of vibrational excitation of N_2 .

B. Molecule–Molecule Collisions

In high-temperature relaxation of air behind strong shock waves, the population of NO is usually relatively small, on the order of 5–10%. Still, available data, even though limited [81], indicate that NO - NO collisions could be a noticeable factor in vibrational relaxation of NO , especially at low to moderate temperatures, due to fast vibrational relaxation times. Comparison of the vibrational relaxation times for this collision, used in different solvers, is given in Fig. 2a. The DSMC solver uses LB model for this interaction, with the relaxation time approximating that of Ref. [81]. The temperature dependence in this case is relatively weak. It is even weaker in STS, where the FHO model is used with parameters that provide reasonable fit to the existing data. Both NS solvers apply the same Millikan–White–Park correlation, with the result denoted as “NS.” The ME solver does not take into account NO - NO collisions, and thus it is not given here. Generally, similar to the earlier comparison, there is

large difference between the relaxation times, and new accurate theoretical and/or experimental data would be necessary to resolve that difference.

The collision type that has a large impact on the thermal and chemical relaxation behind a strong shock wave in air is $O_2 + N_2$. It is a major contributor to the vibrational excitation and subsequent dissociation of O_2 , and thus examined here (Fig. 2b). The NS solvers use the conventional Millikan–White correlation, with somewhat different coefficients in the Park’s high-temperature correction, so that the relaxation time at higher temperatures is lower in LeMANS than in SU2-NEMO. For the DSMC solver, two different models are shown here. The first, used in the high-fidelity DSMC-M2 approach, is 3D FHO, with Morse parameters chosen to realistically describe [46] this interaction. The temperature dependence of the relaxation time for this model is fairly close to that of SU2-NEMO. The second model is based on the discrete LB method, but the traditional Millikan–White expression in that case is replaced by the temperature dependence recommended in the recent experimental study [12]. As discussed in detail in Ref. [12], the measured vibrational temperature dependence on time in the reflected shock wave in air suggests that the relaxation of O_2 on nitrogen may be significantly slower than that

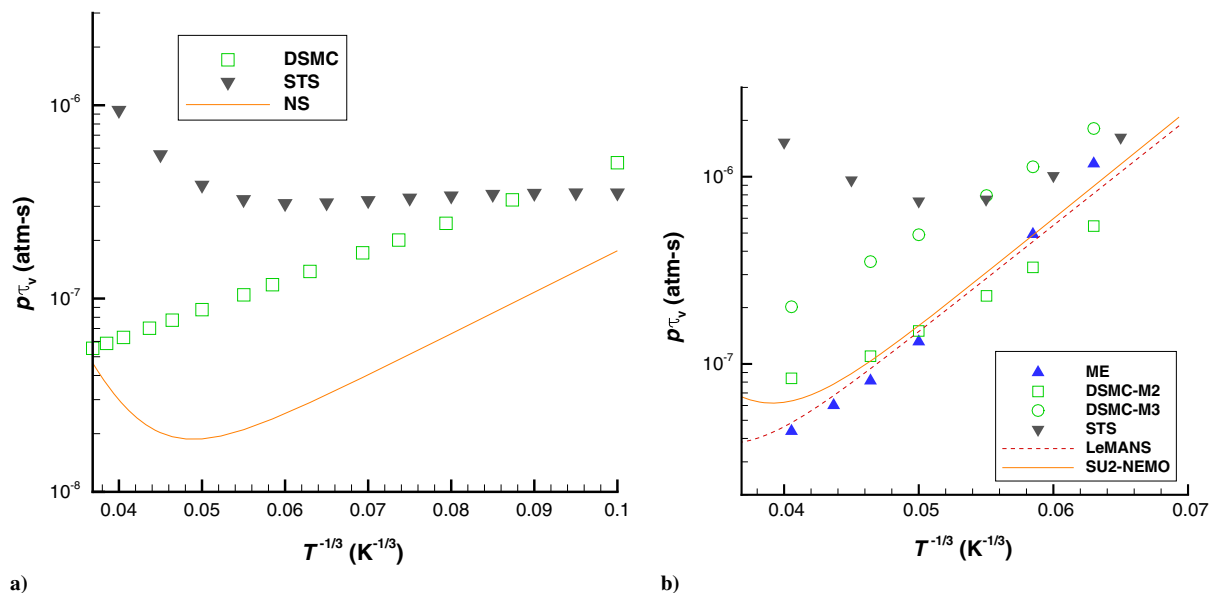


Fig. 2 Vibrational relaxation time for NO - NO (a) and $O_2(v) + N_2$ (b) collisions.

of Millikan–White–Park. This is clearly seen in Fig. 2, with the VT relaxation approximately a factor of three slower for DSMC-M3 than DSMC-M2. The LB algorithm prohibiting double relaxation, used in this work, was shown earlier to accurately capture the prescribed temperature dependence of the vibrational relaxation time at thermal equilibrium, and thus DSMC-M3 matches that of Ref. [12]. Note, however, that the oxygen vibrational temperature was evaluated [12] from the populations of lower vibrational levels (less than 7), and therefore the shown relaxation time may not accurately represent the relaxation of higher vibrational levels, which are expected to make disproportionately large contribution to the dissociation rate. In addition to the energy transfer between vibrational and translational energy modes, there is also VV transfer, which may significantly impact the vibrational energy relaxation of oxygen. Experimental studies [12] have shown that while the VV energy transfer is important at low temperatures, its impact decreases as the gas temperature increases, and so it could not be detected above 6000 K. In this work, only the DSMC-M1 model takes into consideration the VV energy exchange, and its effect on the results of the computations will be discussed below.

V. Equilibrium Reaction Rate Constants

A. Dissociation Reactions

Let us now compare the dissociation reaction rate constants used in different solvers for the key reactions involving O_2 and NO species. For the $N_2 + O_2 \rightarrow N_2 + O + O$ dissociation, Fig. 3a, there is a reasonable, within a factor of two, agreement for temperatures above 6000 K for most solvers. The exception here is STS, for which the rate constant is several times faster. At lower temperatures, the difference is somewhat larger, but the dissociation is expected to be of lesser importance in that regime. This is because inside a hypersonic shock, where the temperature is rising quickly, there is not enough time for significant vibrational excitation and dissociation. And downstream from the shock front, in the hot layer where the temperature gradually decreases, there are often few oxygen molecules left and, moreover, the flow is typically dominated by the exchange reactions.

The rate constant for the collisional dissociation of nitric oxide by atomic oxygen, shown in Fig. 3b, indicates significantly larger differences between the solvers, and mostly between the conventional continuum and the state-specific. The rate constants for ME, DSMC, and STS, based on various QCT and experimental data sets (see the discussion in Ref. [21]), agree well, within approximately 40%, for all temperatures considered here. The continuum solver rate constants are considerably larger. The difference is approximately a factor of three for SU2-NEMO, which uses Ref. [79], and up to two orders of magnitude in LeMANS, based on recommendations of

[55]. For the NO dissociation by N_2 (not shown here because its rates are over an order of magnitude lower than those of $NO + O$, and thus it is somewhat less of a factor), the rate constant in LeMANS is on average 10 times higher than in the state-specific approaches, whereas in SU2-NEMO, it is over 20 times higher. Generally, there are large uncertainties in NO dissociation rates, and the discrepancies between the numerical approaches reflect these uncertainties. New, reliable data on these reaction rates are therefore highly desirable, especially for collisions with O and N_2 . While the NO dissociation rates are expected to be lower than those of the exchange reactions, significant heat removal in these reactions may impact the overall gas temperatures, as will be shown below.

B. Exchange Reactions

Exchange reactions are expected to be the primary source of NO at most flow conditions examined in this work, and thus the corresponding reaction rate constants are compared below. Only the two reactions that produce NO are shown here. These should still be indicative, because the equilibrium constants, which represent the ratios of the forward and reverse reaction rate constants, are fairly close in the considered solvers (see also the discussion and results in Ref. [7]). For both NS solvers used here, the results are presented with the equilibrium constants obtained by the Gibbs free energy approach to calculating backward reactions. This approach was found to produce results almost indistinguishable from those based on Park’s polynomial expansions of thermodynamic properties [55]. The latter ones are fairly close to the NASA recommendations [56], which were assumed in DSMC. All these polynomial expansions used for thermodynamic properties of real gases are taking into account the excitation of the electronic degrees of freedom. In the baseline STS solver, the electronic degrees of freedom are not included, and the reverse rates constants for recombination reactions are obtained from the detailed balance relationships. The model is therefore fully self-consistent, but that also results in equilibrium constants that differ from those obtained using standard thermodynamic databases. Because of that, additional computations were also conducted based on the thermodynamic properties of Ref. [56].

The reaction rate constants for the $O + N_2 \rightarrow NO + N$ reaction are given in Fig. 4a. LeMANS and SU2-NEMO codes both use the results of the QCT calculations [82], and thus their rate constants, labeled “NS,” are identical. The DSMC solver uses an Arrhenius fit to the experimental data [80]. In the ME, the QCT approach is used to obtain the state-specific rates, based on the most recent potential energy surfaces of Truhlar et al. [88]. In the STS solver, the rate constants for the exchange reactions are defined as discussed in Refs. [32,66]. There is good agreement between QCT-based rate

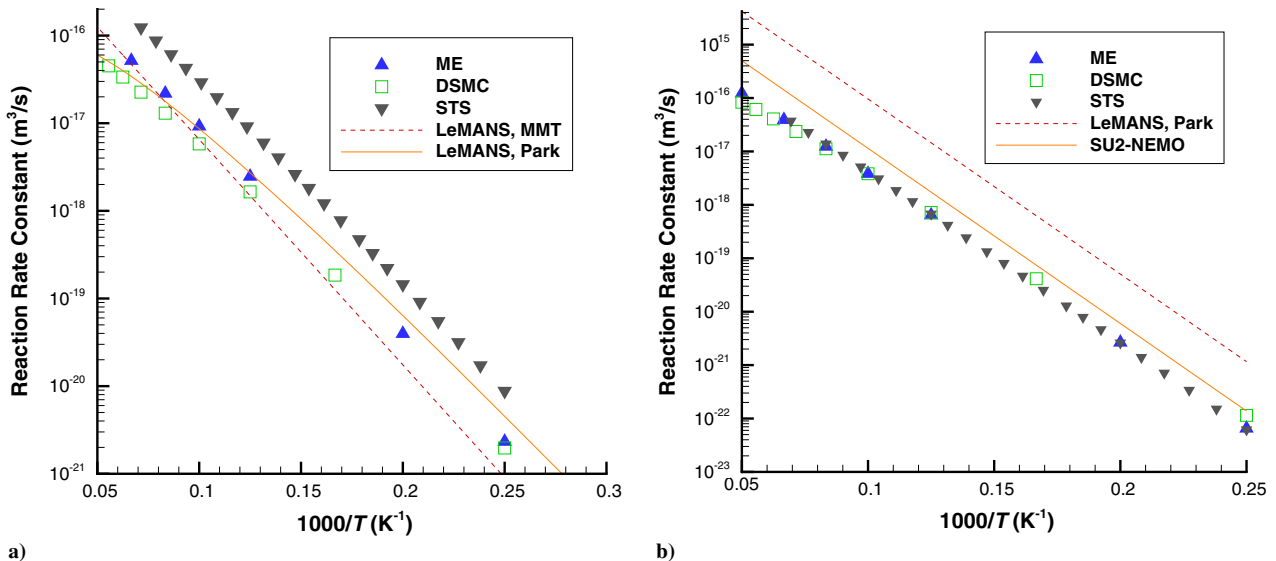


Fig. 3 Dissociation reaction rate constants for $N_2 + O_2$ (a) and $O + NO$ (b) collisions.

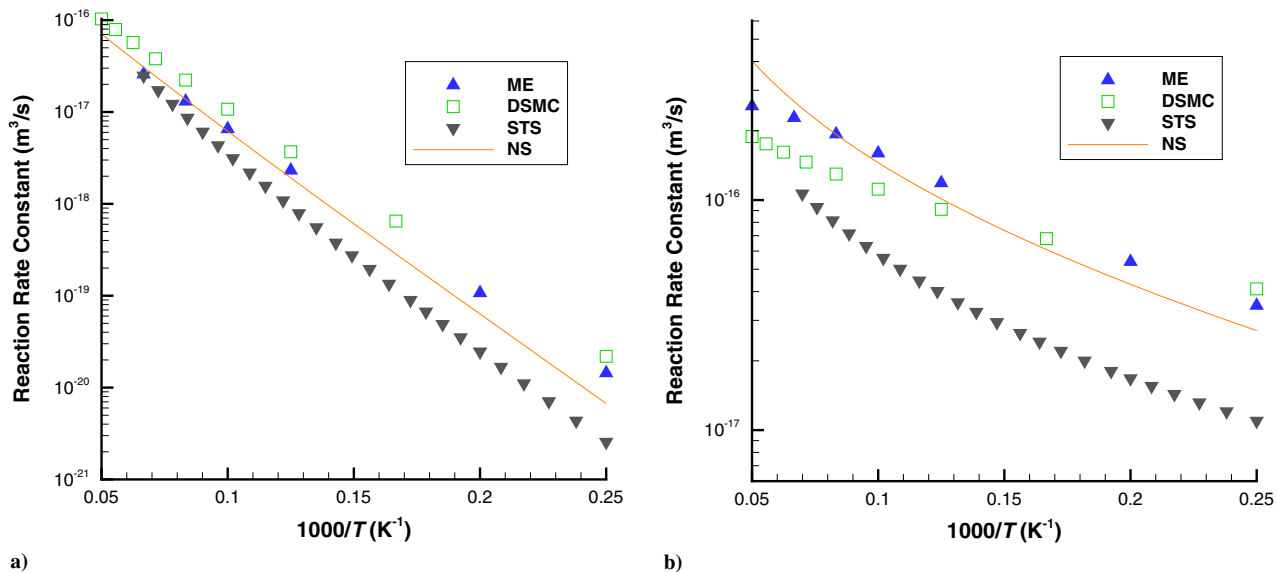


Fig. 4 Exchange reaction rate constants for $O + N_2$ (a) and $N + O_2$ (b) collisions.

constants, NS and ME. The DSMC rate constant is approximately a factor of two higher than QCT, whereas STS is a factor of two lower. For the $N + O_2$ reaction, Fig. 4b, all rates are fairly close, with the exception of STS, which is approximately a factor of two to three lower. Good agreement between the exchange reaction rate constants means that these reactions should not be expected to be a significant factor in any difference observed in flow results obtained by different solvers (again, with the only exception of STS).

VI. Moderate-Temperature Regime

A. Reflected Shock Wave and Comparison with Measurements

Significant differences in vibrational relaxation times and dissociation reaction rates, especially those involving nitric oxide, that were observed for state-specific and fully continuum solvers, are directly related to large error bars and uncertainties associated with these processes. To the best of our knowledge, there are no reliable experimental data that would allow us to conclude which solver or solvers better capture the actual rates. Ideally, one would need a comprehensive database covering the range of temperatures of interest where the macroscopic properties of air species are determined as a function of time with high accuracy. In reality, though, to define reaction and relaxation rates, modelers often have to rely on older experiments where error bars are largely unknown, or more recent QCT datasets where uncertainties such as those related to the complexity of multiple-channel potential energy surfaces as well as large parameter space, significantly complicate the analysis. Surface properties measured in high-enthalpy facilities are often being used as the sanity check for the complete flow model, but even a good agreement cannot guarantee the accuracy of each individual species-based collision or reaction model.

The recent and ongoing shock tube experiments may offer the path to closing the knowledge gap and provide the information necessary to reduce the error bars in temperature-dependent reaction and relaxation rates. The measurements [5] of absorption in the Schumann–Runge band inside incident shock waves provided the vibrational temperature and time-dependent UV absorption data, although at this time, only in oxygen shock waves. Recent experiments conducted in NASA EAST shock tube [83] offer unique spectrally resolved data in 190–1450 nm range in air for incident shock velocities of 7 km and higher, although direct comparison and model validation could be somewhat complicated. This is because the emission data make it necessary to compute the properties of excited electronic species or make additional assumptions on these species. A different approach was used in the recent study [12,84] where the UV absorption of O_2 has been measured inside reflected shock waves in air. High-accuracy analysis of nonequilibrium relaxation of molecular oxygen species at

temperatures up to 14,000 K provides an excellent opportunity for model and rate validation.

It has to be noted, however, that a time-accurate one or 2D approach, similar to that proposed in Ref. [20], is necessary to model the time-dependent relaxation behind a reflected shock that captures both the development of the boundary layer at the side wall and the mass, momentum, and energy transfer in the direction of the propagating shock wave. Such an approach is currently available only in the DSMC solver, and the correct relaxation cannot be reproduced in a standard 0D bath suitable for the other solvers used in this work. This is illustrated in Fig. 5a, where the time relaxation of translational and vibrational temperatures computed in DSMC is shown for a 0D adiabatic heat bath and a 1D incident shock reflection recorded at a distance of 5 mm from the end wall, similar to the experiments [12]. Here, the 1D time axis was translated such that the translational–vibrational equilibrium is reached at approximately the same time in 0D and 1D. In 1D, the velocity of the incident shock wave, propagating in a 32-Torr room-temperature air, was set at 2.52 km/s to reproduce one of the experimental conditions [12]. In this case, the translational–rotational temperature and pressure of the gas immediately after the reflected shock was calculated in Ref. [12] as 7230 K and 32 Torr, respectively, under the assumption of no vibrational excitation and dissociation at that point. This condition was therefore assumed in the 0D calculation.

There are several conclusions that may be drawn from Fig. 5a. First, the relaxation before the peak vibrational temperature is much slower in 0D, obviously due to the neglected effects of nonzero bulk velocity in the reflected shock, and energy transfer from the hotter downstream region in the presence of sharp spatially varying thermal gradients. The values of the maximum vibrational temperature are nearly the same in 0D and 1D, both for oxygen and nitrogen. Finally, the after-peak relaxation proceeds similarly in 0D and 1D, likely because the bulk velocity becomes close to zero, and thermal gradients are lower than at earlier time moments. Most of chemical reactions occur when there is significant excitation of the internal degrees of freedom of molecules. This explains fairly similar slopes of atomic oxygen and nitric oxide mole fractions in 0D as compared to 1D, as shown in Fig. 5b, even though the 1D profiles lag behind those in 0D.

Let us now compare the computed and experimental vibrational temperatures of O_2 . This comparison is presented in Fig. 6a, where three different DSMC models are given. Note that the O_2 vibrational temperature for DSMC-M4 is close to DSMC-M3, and thus not shown here. The DSMC-M1 model does not have a pronounced peak, which is due to the large effect of the VV energy transfer between the O_2 and N_2 molecules in that model. It was found in

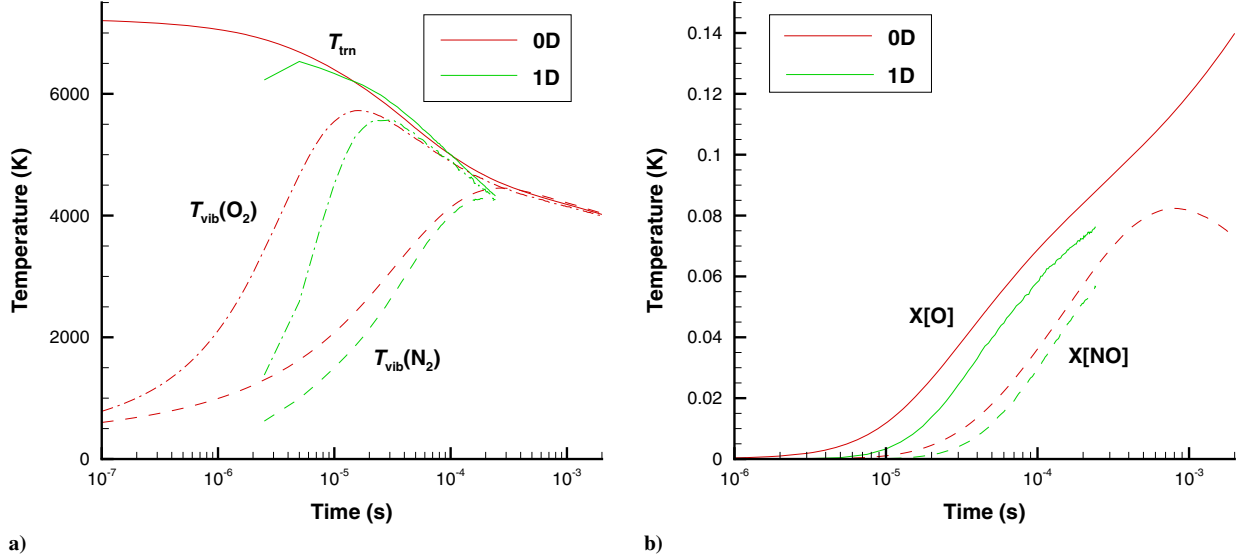


Fig. 5 Comparison of time evolution of temperature (a) and mole fraction (b) gas properties in 0D adiabatic heat bath and 1D reflected shock wave.

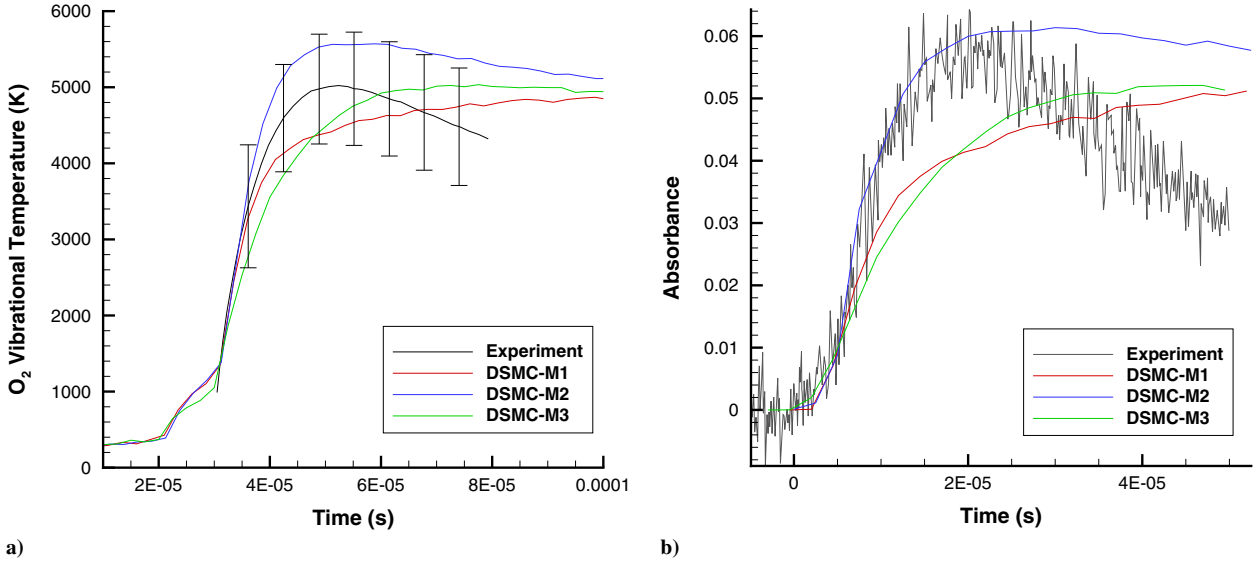


Fig. 6 Measured and computed vibrational temperature of O_2 (a) and absorbance (b) through the reflected shock.

Ref. [12] that the actual impact of VV transfer is small at these conditions, and the temperature dependence of the VV relaxation number used in the DSMC-M1 model likely requires reconsideration. The temperature obtained with the DSMC-M2 model, where the VV energy transfer was turned off, is closer to the experimental result than the two others. The maximum is overpredicted in DSMC-M2, but still within the experimental error bars (and that difference could also be offset partially if VV transfer were included in DSMC-M2 with relaxation times slower than in DSMC-M1). The most significant difference between the experiment and DSMC-M2 comes after the peak, where the measured decrease in the vibrational temperature is much faster than the computed one. The reasons for this difference are not known to the authors at this time, but most likely are related to oxygen dissociation or exchange reaction rates. Interestingly, the initial relaxation in the DSMC-M3 model, which is based on the vibrational relaxation times recommended in Ref. [12], is visibly slower than in the experiment; it is not currently clear why there is such a difference.

Our earlier comparison [85] of $T_{\text{vib}}(O_2)$ with measurements [5] has demonstrated that it is beneficial to compare not only vibrational temperatures, but also absorbance traces. This has also been done in this work, with the measured versus computed absorbance versus

time dependence shown in Fig. 6b. The NEQAIR code [86] was used in these computations, with input flow properties taken from the corresponding 1D reflected-shock DSMC runs. The comparison with Ref. [12] is conducted for a wavelength of 236.9 nm. Comparison of the measured profile with DSMC-M2 shows that they are very close up to the peak; after that, the measured absorbance decreases much more rapidly than computed, similarly to what was observed for the vibrational temperature. DSMC-M1 and DSMC-M3 differ noticeably from the experiment during the initial relaxation, at the peak, and in the after-peak relaxation.

B. 7230 K Adiabatic Heat Bath

Now examine the adiabatic relaxation in a 0D heat bath under the initial conditions considered in the previous section, with results obtained by the five computational solvers used in this work. Note first that the continuum solvers LeMANS and SU2-NEMO traditionally assume a single vibrational temperature, even though that temperature is being affected through separate vibrational paths of molecular species. Therefore, only ME, DSMC, and STS results may be compared to the reflected shock measurements, although indirectly due to the lack of spatial effects in 0D. Hereafter, the notation “DSMC” is used for the DSMC-M2 model. The vibrational

temperatures of O_2 are shown in Fig. 7a. The figure shows that the vibrational relaxation of O_2 is fairly close in the DSMC and ME methods. The reason for this is that the vibrational relaxation in this case proceeds at a translational temperature of about 7000 K. As illustrated in Fig. 2b, the ME and DSMC vibrational relaxation times at this temperature are very close for the O_2 - N_2 collisions, which is the primary collision for O_2 vibrational relaxation in this temperature regime. The $T_{\text{vib}}(O_2)$ relaxation for STS is approximately two times slower than in DSMC, which is also consistent with the vibrational relaxation times plotted in Fig. 2b. The peak $T_{\text{vib}}(O_2)$ in STS is over 1000 K lower than in DSMC and ME, which is attributed to fast O_2 dissociation as will be shown below. The experimentally deduced [12] peak vibrational temperature of 5000 K lies approximately between those of ME and DSMC, and STS. DSMC (and thus ME) is likely more accurately predicting the location of the peak (cf. to Fig. 6a). After-peak relaxation is similar in the three approaches, which implies that all three would underpredict the measured fast decrease of the vibrational temperature after the peak.

The nitrogen vibrational temperatures computed by the three solvers, also shown in Fig. 7a, are much closer than those of oxygen. The explanation for this is that the primary mechanism of the excitation of nitrogen vibrational modes under these conditions is the VT energy transfer in N_2 - N_2 collisions, and these three approaches have vibrational collision times that are close to each other—and to the Millikan–White expression, for temperatures in the 5000–8000 K temperature range. Note that after approximately 10 μs relaxation time, STS gas temperature is somewhat lower than in DSMC. This is related to the delayed oxygen dissociation in DSMC as a result of strong vibrational favoring assumed in the Bias dissociation model for this species, chosen to better match the most recent QCT results (see the relevant discussion in Ref. [21]). In the absence of experimental confirmation, it is not clear which solver provides better accuracy in that regard.

To compare the vibrational temperatures in the state-specific and conventional continuum approaches, the overall T_{vib} were calculated in ME, DSMC, and STS, with O_2 , N_2 , and NO species temperatures included according to their mole fractions. The result is illustrated in Fig. 7b. Hereafter, “Gibbs P” stands for preferential model of dissociation with Gibbs approach used to calculate the equilibrium constants. Note that while only LeMANS results are shown in this and the following figure, the corresponding SU2-NEMO profiles are nearly identical to LeMANS. The vibrational temperatures for the continuum approaches are very close until approximately 30 μs , when the vibrational temperature for the Gibbs model reaches the translational–rotational temperature. This is because the vibrational relaxation at the earlier stage is driven by collisions between nitrogen and oxygen molecules, and the corresponding VT relaxation

times are all based on the same Millikan–White correlation. The translational–rotational temperature T for the MMT model is the slowest to relax as compared to the other models and approaches. Initially, T for MMT is close to that of DSMC, but start to deviate after about 40 μs . The difference in the relaxation times between MMT and other models becomes quite significant, reaching up to an order of magnitude after 1 ms. Here again, even though the MMT model is based on the most recent QCT results, it is not clear which of the models better reproduces the actual flow due to multiple factors that influence the gas temperature.

As expected, taking into account vibrational favoring in dissociation reactions results in significant delay of dissociation. This effect is clearly visible when comparing the atomic oxygen mole fraction for the preferential Gibbs model with the MMT model, shown in Fig. 8a. While the O_2 dissociation reaction rate constant for the Gibbs model is only a factor of two to three faster than MMT for this range of temperatures (see Fig. 3a), there is approximately an order-of-magnitude delay in the rise of the atomic oxygen mole fraction for MMT. The fastest oxygen dissociation rate is observed in STS and ME solvers, and their oxygen mole fraction profiles are fairly close. There are several factors in play that explain this. STS applies the fastest O_2 dissociation rate on N_2 of all solvers and models used here (see Fig. 3). The initial rise of the oxygen mole fraction is slower in ME due to a somewhat stronger vibrational favoring, but then there is sharp increase in $X[O]$ due to very fast increase in vibrational temperature of O_2 (see Fig. 7), and thus fast $O_2 + O_2$ dissociation [7]. $X[O]$ for DSMC is approximately between STS and MMT profiles. The nitric oxide mole fractions are also shown in Fig. 8a. As will be discussed in detail below, NO is mostly formed and destroyed in the exchange reactions, and because there is now vibrational favoring assumed in these reactions and the DSMC and ME reaction rates (Fig. 4) are close, the corresponding NO mole fraction profiles are also close. NO formation in MMT is significantly delayed because of the lower oxygen dissociation rate, which delays the formation of O that participate in $O + N_2$ exchange reaction. The formation of NO in STS is also delayed, but this is primarily related to the lower NO formation rates assumed in this solver (Fig. 4).

Direct comparison of instantaneous reaction rates applied in different solvers is given in Fig. 8b for the key dissociation reaction. Note that up to approximately 100 μs the relaxation proceeds under significant VT nonequilibrium; after that time, the temperatures mostly equilibrate, although there is still some degree of nonequilibrium present in the population of high vibrational levels of oxygen for state-specific approaches that use vibrationally favored dissociation models. Compare first the time dependence of the oxygen dissociation rates for DSMC and STS. One can see that there is qualitative difference between the two: the STS rate decreases monotonically

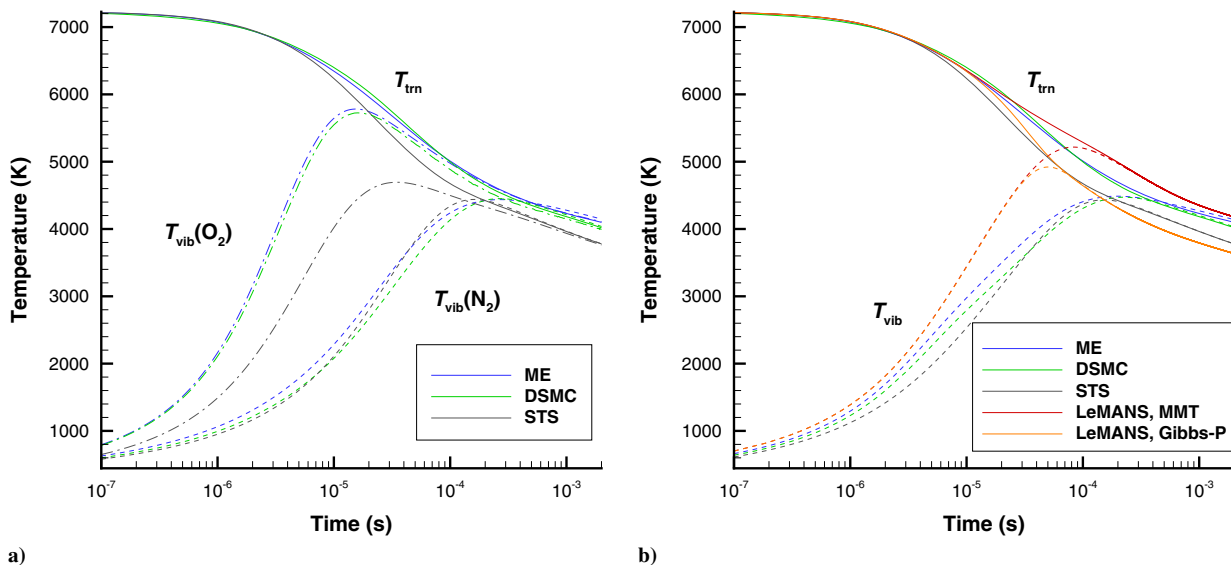


Fig. 7 TC1: species vibrational temperatures (a) and overall vibrational temperatures (b) computed with different approaches.

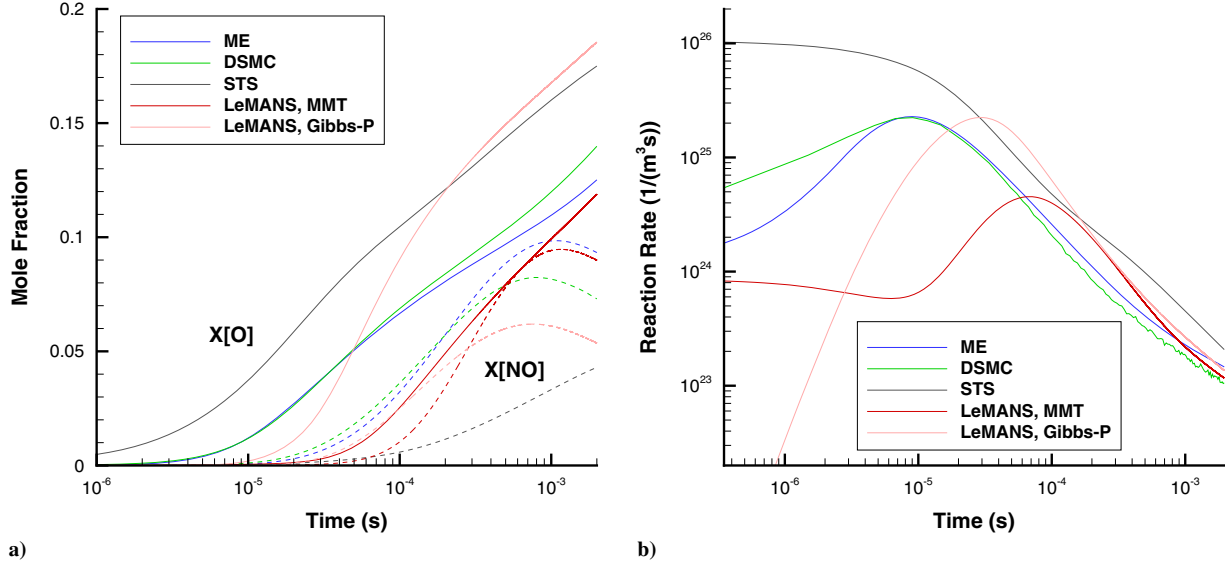


Fig. 8 a) Species mole fractions for different approaches. b) Reaction rates for $N_2 + O_2 \rightarrow N_2 + O + O$.

with time, whereas in DSMC, there is a pronounced peak at $10 \mu s$. The main reason for such a difference is the degree of vibrational favoring assumed in these approaches. In DSMC, it is much higher than in STS, so that the probability of dissociating molecules that reside at low vibrational levels is much smaller. This is especially significant when there is strong vibrational and VT nonequilibrium. For example, in a 15,000 K translation-rotation bath with a low vibrational temperature of 1000 K, only 0.02% of reactions come from the ground level in DSMC, whereas in STS, it is almost 90%. Therefore, under conditions when there is little vibrational excitation, there are very few dissociation reactions in DSMC. Moreover, even those few reactions primarily depopulate higher vibrational levels, further depressing the dissociation rate. The result is the gradual decrease of this rate with time, observed in DSMC. Yet another factor is the dependence of reaction probability in DSMC on the vibrational energy of not only the dissociating molecule, but also its collision partner: reaction probability increases with vibrational level of N_2 ; this dependence is assumed to be negligible in STS.

There is also considerable degree of vibrational favoring present in the QCT-based ME approach, and its initial increase in the reaction rate is more pronounced than in DSMC, although the decrease after the peak is nearly the same. The dependence of the dissociation rate on the vibrational energy is even more significant in LeMANS that uses the Park vibrationally favored dissociation model with preferential dissociation and Gibbs approach to finding equilibrium constants ("Gibbs-P"). In this case, there are almost no reactions at the initial time, but the rate increases many orders of magnitude as the vibrational temperature increases from 300 K to its peak (shown in Fig. 7b). The MMT model has more complex time dependence of the dissociation rate. Over the first few microseconds, there is a weak decrease in the rate, associated with the decrease of gas (translational-rotational) temperature. The increase is weak even though the gas temperature decreases from over 7230 K to less than 6000 K because of the vibrational temperature, which goes up from its initial 300 K to over 2000 K at $3 \mu s$. At longer times, the vibration-dissociation coupling results in the increase of the reaction rate, which reaches its peak at about $80 \mu s$, which coincides with the location of the T_{vib} maximum. After that, the rates decrease with T and T_{vib} . To summarize the instantaneous rate comparison, even for the arguably most important reaction at that temperature regime, there are still large differences, both qualitative and quantitative, between the results obtained. To resolve such differences, experimental studies would be necessary that target specifically oxygen depletion at the early stages of the relaxation.

$O + N_2$ exchange reaction is the primary mechanism that impacts the NO formation during the initial stage of the relaxation, and the difference in the instantaneous reaction rates in this case (not shown

here) is qualitatively similar to that observed for the NO mole fractions. The ME and DSMC rates are fairly close, whereas STS is significantly lower, with the exception of the first microsecond, where the high exchange reaction rate in STS is due to larger mole fraction of O produced after O_2 dissociation.

To better understand the complex nature of chemically reacting, nonequilibrium air relaxation, and the impact of different reaction mechanisms, it is useful to compare the relative contribution of these mechanisms to the depletion or formation of atomic and molecular species, and also to the gas temperature decrease over time. Such contributions are considered here for the two numerical solvers where results differ significantly, DSMC and STS, and two primary UV observables, molecular species O_2 and NO. The rates of reactions that directly impact the density of molecular oxygen in the DSMC method are plotted in Fig. 9a. Minor contributors that change the overall rate by less than 1% are not shown. The reaction contributions that decrease and increase the density of O_2 have negative and positive values on the Y axis, respectively. The dissociation and recombination reactions are combined here, although the recombination effect is almost negligible; the exchange reactions are plotted separately. Over the first $10 \mu s$, the dissociation reactions dominate, with the largest factor being the dissociation on N_2 molecules. Increase in dissociation rates results in decreasing gas temperature, which then decreases those rates (approximately $30 \mu s$). At that time, exchange reactions start playing a bigger role, especially that with atomic nitrogen. As more nitric oxide is produced, the contribution from the reverse exchange reaction $O + NO$ also becomes significant and, later, comparable to the forward reaction. The exchange reactions predictably control the population of nitric oxide, as shown in Fig. 9b. The NO dissociation-recombination effect is negligible and thus not shown. Interestingly, even though the N mole fraction is very small, it is still sufficient for the two NO producing reactions to have nearly equal contribution for most of the relaxation time. Their contribution increases in the first $100 \mu s$, and then decreases with gas temperature.

The instantaneous reaction rates from different paths that have noticeable effect on the molecular oxygen density in the STS approach are shown in Fig. 10a. In this case, the dissociation on N_2 totally dominates (note that the Y axis was split to better illustrate the contribution from other reactions). $O_2 + N_2$ dissociation rate decreases monotonically with time, but only after $100 \mu s$ it becomes comparable to the other rates. At later times, the contribution from the nitric-oxide-forming exchange reaction becomes larger, but the effect of dissociation is still significant, especially if the reverse exchange reaction is accounted for. Clearly this is qualitatively different from DSMC, where the overall contribution of dissociation and exchange was comparable. For the NO density, similar to DSMC, the exchange reactions are the main factor, and the effect of dissociation is

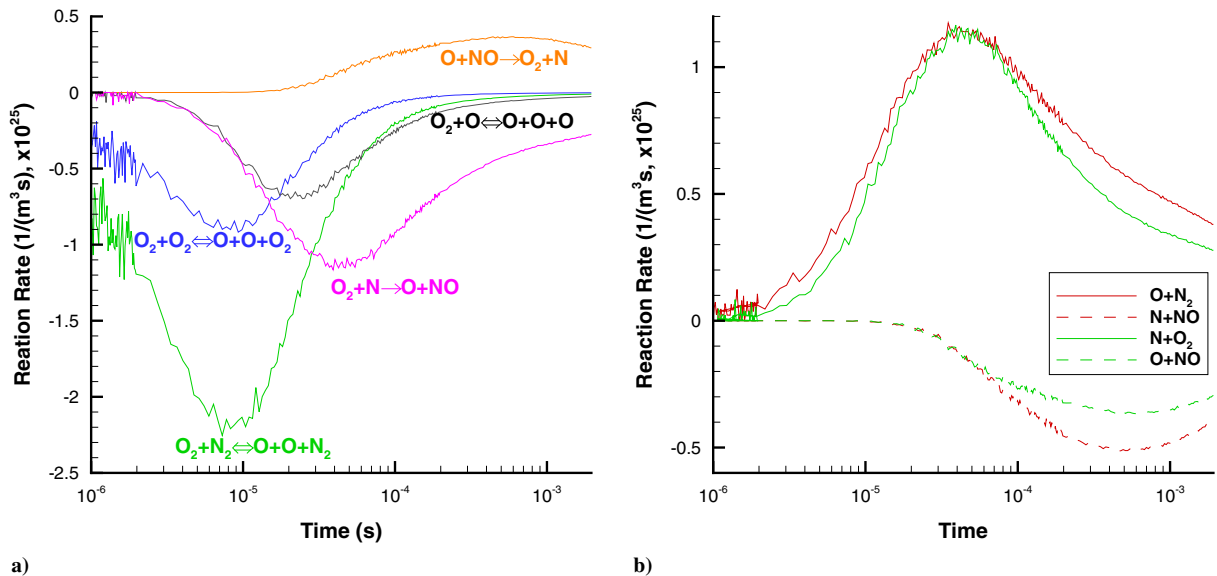


Fig. 9 TC1: contribution of different reaction rates to O₂ (a) and NO (b) density change (DSMC-M2).

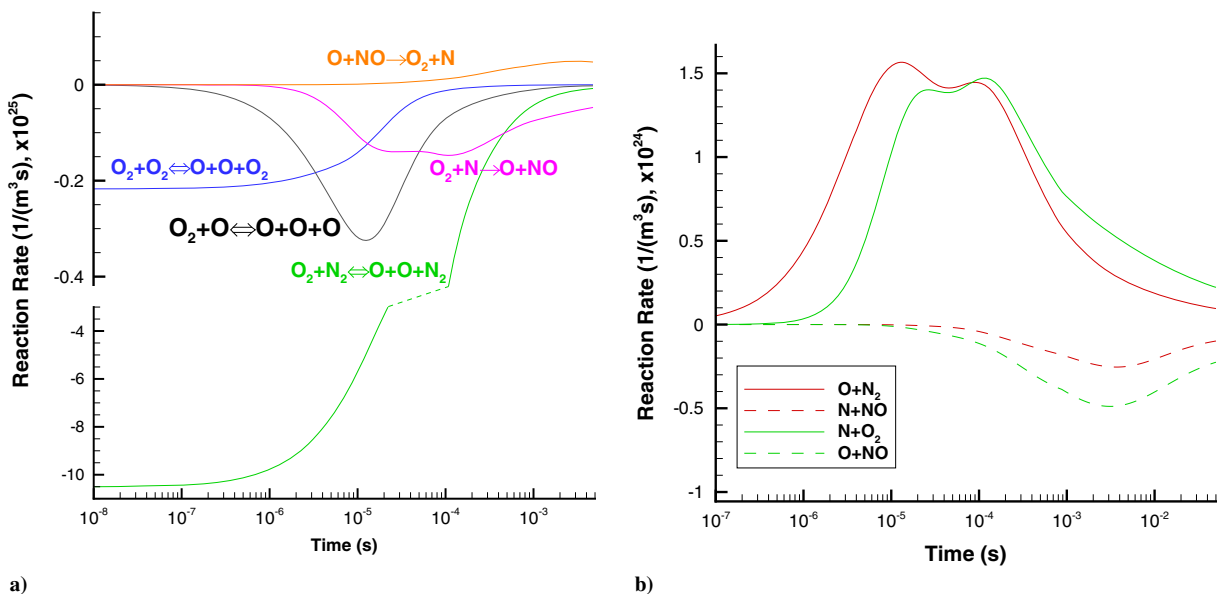


Fig. 10 TC1: contribution of different reaction rates to O₂ (a) and NO (b) density change (STS).

negligible (Fig. 10b). Note that the profiles for the NO formation reactions have two peaks. Such a nonmonotonic change in the forward reaction rates is likely a combined effect of the decreasing temperature, and thus forward reaction rates, due to dissociation, and the sharp increase in the number of atoms due to this dissociation, which increase the number of exchange reactions. The reaction rate for O + N₂ increases earlier than in DSMC due to fast oxygen dissociation discussed earlier. At the end of the simulations, there are many more N + O₂ reactions than O + N₂, even though both are equilibrated by the reverse reactions. It is opposite in DSMC, and the difference is attributed to equilibrium constants that do and do not include the electronic excitation in DSMC and STS, respectively.

The exchange reactions were found to have little combined effect on the decrease in gas temperature over time in STS. This is illustrated in Fig. 11a, where all noticeable contributors are given. The contribution of the O + N₂ exchange reaction versus time never exceeds 25%, whereas the N + O₂ reaction contribution is negligible and thus not shown. Almost all of the remaining temperature change comes from N₂ + O₂ oxygen dissociation,

which dominates throughout the relaxation. This was found not to be the case in DSMC, presented in Fig. 11b. While the N₂ + O₂ reaction is the most important for the first 40 μs, the O + N₂ exchange reaction contributes more at longer times. Same for O + O₂ dissociation, which starts to contribute after 1 μs, and its relative contribution increases significantly with time. Note that all dissociation reactions have well-defined peaks in their relative contributions. For the dissociation on O, this is primarily related to the gradual increase in the atomic oxygen mole fraction, resulting in more reactions, and decrease in temperature, which decreases the reaction rates. For dissociation on O₂ and N₂ molecules, the initially low numbers of reactions are related to strong vibrational favoring assumed in DSMC. Initially low vibrational excitation of molecules significantly reduces the number of reactions as compared to a thermally equilibrium bath at this temperature; successive vibrational excitation strongly increases the number of reactions. Note that the peak in the rate of temperature change due to N₂ + O₂ oxygen dissociation reaches approximately 10⁻⁷ in DSMC, thus over six times weaker than what is initially

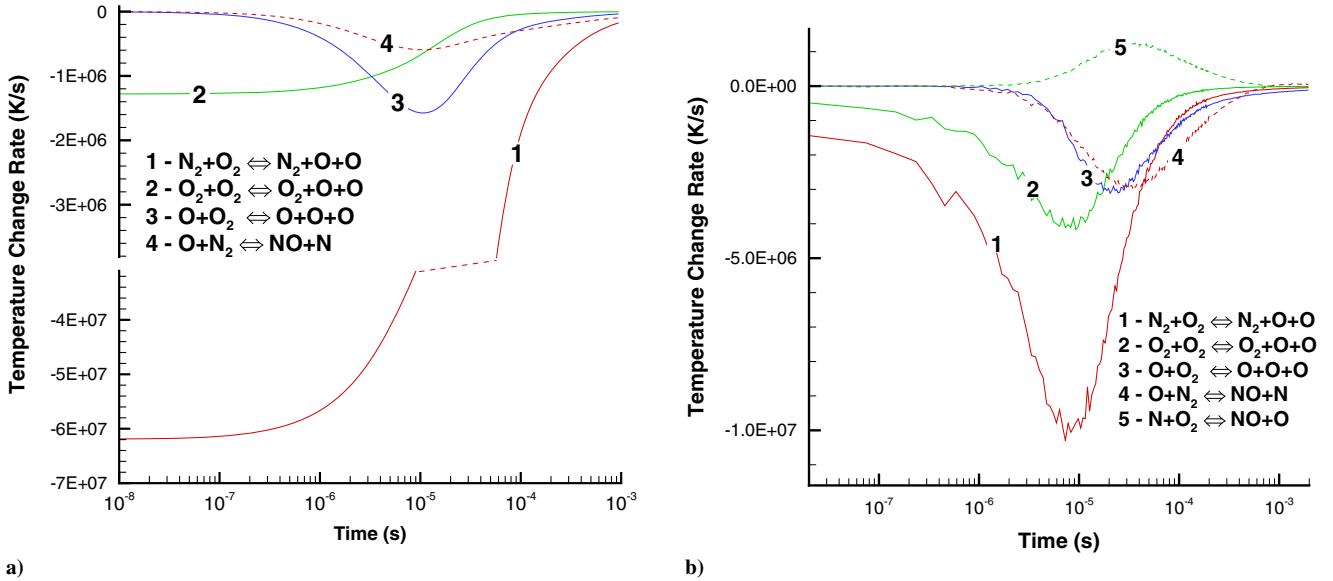


Fig. 11 TC1: impact of reaction channel on the rate of temperature change for STS (a) and DSMC-M2 (b).

observed in STS. The resulting temperature change is similar, though, because the temperature in DSMC decreases over a longer time due to the exchange reactions.

VII. High-Temperature Regime

A. 15,000 K Adiabatic Heat Bath

The temperature conditions considered in the previous section correspond to the highest incident shock velocity of experiments [12] where the thermal relaxation results were published. The ongoing enhancements in the instrumentation, although challenging, carry the promise of reaching significantly higher velocities, and thus temperatures in the reflected shock, possibly as high as has been achieved most recently in Ref. [84], where the temperatures as high as 14,000 K were observed in oxygen–argon shocks. Reaching such temperatures will essentially create thermally and chemically relaxing flows under conditions similar to those behind hypersonic shocks in high-enthalpy shock tunnels such as HEG, Hypervelocity Expansion Tube (HET), and T6, thus bridging shock wave and shock tunnel conditions. Flows at such high temperatures are characterized by nearly complete dissociation of oxygen, and noticeable dissociation of nitrogen. Direct comparison of the numerical solvers applied

to nitrogen dissociation in a high-temperature adiabatic bath conducted in our previous work [7] has shown that the results obtained by different approaches, in particular gas temperature and nitrogen atom mole fraction, are reasonably close, and therefore the main focus of this work is the NO species, as well as oxygen. In this section, we consider at the initial translational–rotational temperature of 15,000 K and vibrational temperature of 300 K, with the initial gas number density of 10^{25} m^{-3} . Such a relatively large density was chosen to have observable effect of recombination, so that the steady state can be reached in all calculations.

High temperatures and fast reactions amplify differences not only between computational solvers, but also between flow models used in each solver. To illustrate this, the model effect is shown in this section for the fully kinetic and continuum approaches. The overall translational temperature and the oxygen vibrational temperature computed with the four models used in this work in the DSMC method (see Sec. III.A) are presented in Fig. 12a. Several conclusions may be drawn from this comparison. The first is the VV model specific: the peak oxygen vibrational temperature in DSMC-M1, which includes VV, is somewhat lower than in no-VV DSMC-M2. The lower maximum value of O_2 vibrational temperature is due to the energy transfer from oxygen to nitrogen vibrational modes during the VV transfer.

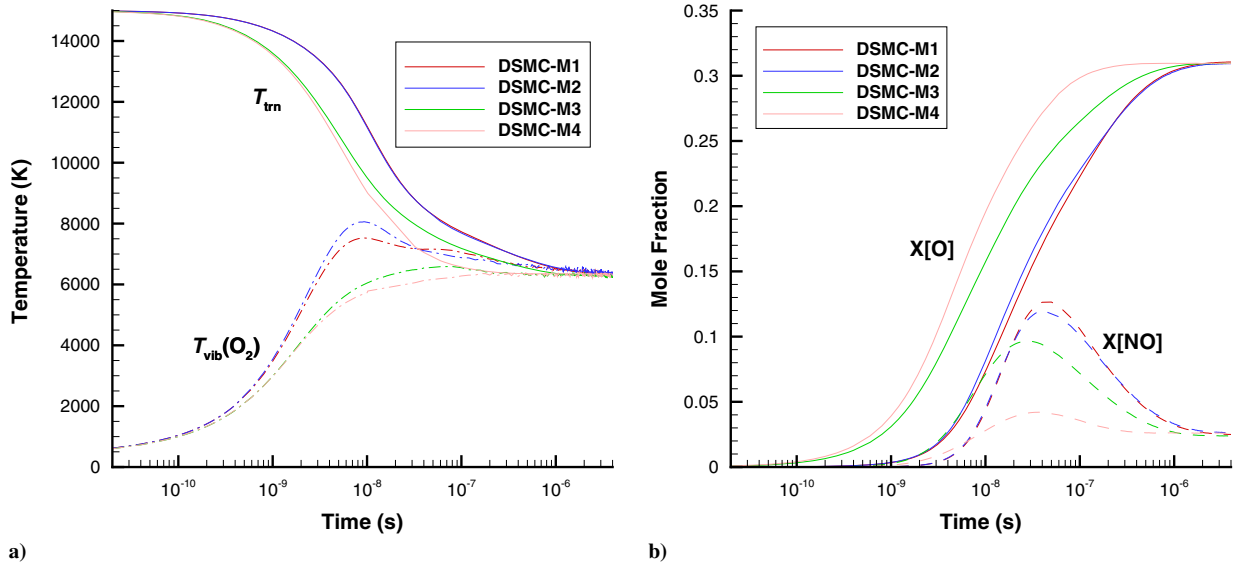


Fig. 12 TC2: impact of DSMC gas model on temperatures (a) and mole fractions (b).

This may be an additional indication that the temperature dependence of the VV relaxation number may need to be reconsidered, because experimental studies [12] provided an indication of significantly diminished impact of VV at temperatures higher than 6000 K. Note that even for a fast VV relaxation of DSMC-M1, there is little impact on the translational temperature, because this energy transfer is near-resonant and thus confined to the vibrational modes of O_2 and N_2 . There is also little impact of VV on dissociation, which implies that the populations of higher vibrational levels are driven at this temperatures mostly by the VT transfer. The vibrational favoring of dissociation in DSMC-M2 results in significant delay of chemical relaxation, as compared to the TCE dependence of the reaction cross sections in DSMC-M3. This is clearly manifested in the translational temperature profiles, where the initial decrease is driven by the heat removal after dissociation. For example, in model DSMC-M3, it takes only 3 ns for the translational temperature to decrease from its initial 15,000 to 12,000 K, whereas in model DSMC-M2, this relaxation takes nearly 8 ns. Finally, thermal relaxation for the QCT-based reaction rate set of DSMC-M3 is similar to Park-based DSMC-M4 initially, but then significantly, by nearly an order of magnitude, deviates from it as the gas temperature decreases below 10,000 K. The primary reason for such deviation is slower dissociation of molecular oxygen in DSMC-M3, as illustrated by comparing atomic oxygen mole fractions in Fig. 12b. As noted earlier, the dissociation of vibrationally favored models is delayed by a relatively slow vibrational excitation of O_2 . Comparing the mole fractions of nitric oxide, one can see that the impact of VV on the peak $X[NO]$ is negligible (compare DSMC-M1 and DSMC-M2), whereas the faster reactions in DSMC-M3 are decreasing the gas temperature, and thus peak $X[NO]$, due to lower rates of NO-producing exchange reactions. Most significantly, the NO population is much lower when Park reaction rate constants are used. This, as will be discussed in more details below, is a combined effects of lower gas temperature due to faster dissociation of oxygen, significantly higher NO dissociation rates, and slightly lower NO producing exchange reaction rates.

Consider now the model effect in the NS solver LeMANS. Comparison of the translational-rotational and vibrational temperature for this case is shown in Fig. 13a. Here, two approaches to the calculation of the reverse reactions rate constants are used, Gibbs and Park's, as discussed in Sec. III.D. For each approach, both preferential and nonpreferential dissociation (more specifically, vibrational energy removal) models are applied, denoted as "P" and "NP," respectively. The reverse reaction rates model has little impact on gas temperatures, essentially making results indistinguishable at this scale; therefore, only one of them (Gibbs) is shown. The difference between the models, although not as large as in DSMC, is still quite

significant. The preferential vibrational energy removal after dissociation results, as expected, in lower vibrational energy for Gibbs-P, with the difference increasing over time and reaching a maximum of about 1500 K near the peak T_{vib} . Lower T_{vib} for Gibbs-P corresponds to visibly higher translational temperature. Note also that T_{vib} becomes noticeably higher than T in Gibbs-NP. There are two factors in play that cause this effect. First, in the nonpreferential dissociation model, it is assumed that molecules are destroyed or created at the average vibrational energy of the cell. The high energy of dissociation E_d removed after each dissociative collision implies that this energy, which is significantly higher than the average energy of molecules in the flow, is primarily removed from translational and rotational energy modes. The second factor causing $T_{vib} > T$ is a relatively slow relaxation of vibrational energy, primarily due to high τ_v of N_2 . This $T_{vib} > T$ effect is absent for the Gibbs-P model, where the vibrational energy removed after dissociation is assumed to be $0.3E_d$, and thus much higher than in Gibbs-NP. The temperatures for the MMT model are initially close to those of the traditional models. However, after a few nanoseconds, the translational and then vibrational temperature become higher. This is related to the dissociation model in MMT, in particular, oxygen dissociation on N_2 . The much slower oxygen dissociation in MMT is illustrated in Fig. 13b, where the atomic oxygen and nitric oxide mole fractions are given. $X[O]$ reaches its equilibrium value approximately four times faster in Gibbs-NP than in MMT. $X[NO]$ are fairly close in all three models, mostly because both preferential energy removal and MMT reaction rates are only applied to dissociation, whereas $X[NO]$ mostly depends on the exchange reaction rates. Therefore, the model impact on NO species propagates only through gas temperature.

In the solver-to-solver comparison given below, we use MMT and DSMC-M2 models of LeMANS and SMILE, respectively, as those are believed to be the most accurate in this case. The translational-rotational T_{trn} and vibrational T_{vib} temperatures computed with all five computational tools are presented in Fig. 14. For the sake of consistency, STS calculation shown here was conducted with the equilibrium constants that include the electronic degrees of freedom, so that the thermochemically equilibrium state is the same for all approaches. The SU2-NEMO temperatures, shown here for the preferential dissociation model, were found to be very close to those of LeMANS (not shown, compare also to Fig. 13a). The initial relaxation of the vibrational temperature was found to be faster in both continuum solvers than in all three state-specific approaches. The main reason for this is fast VT relaxation assumed in LeMANS and SU2-NEMO for O_2 - O_2 and N_2 - N_2 collisions. ME approach has approximately two times higher vibrational relaxation times for these interactions at 15,000 K, but the fast VT relaxation in N_2 - O_2

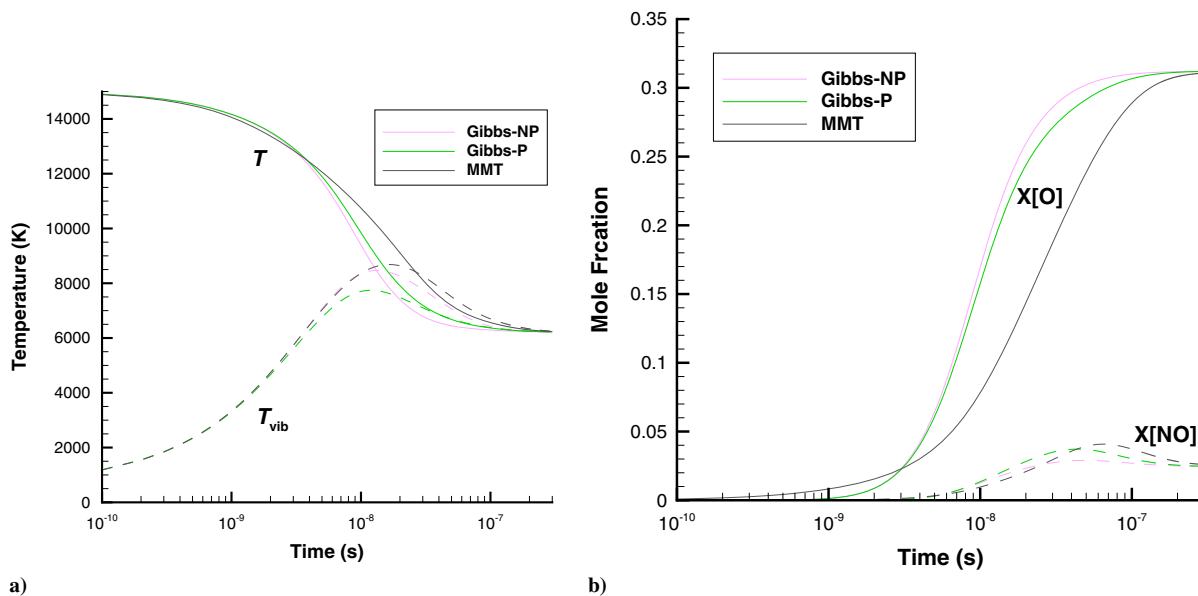


Fig. 13 TC2: impact of Navier-Stokes (LeMANS) reaction model on temperatures (a) and mole fractions (b).

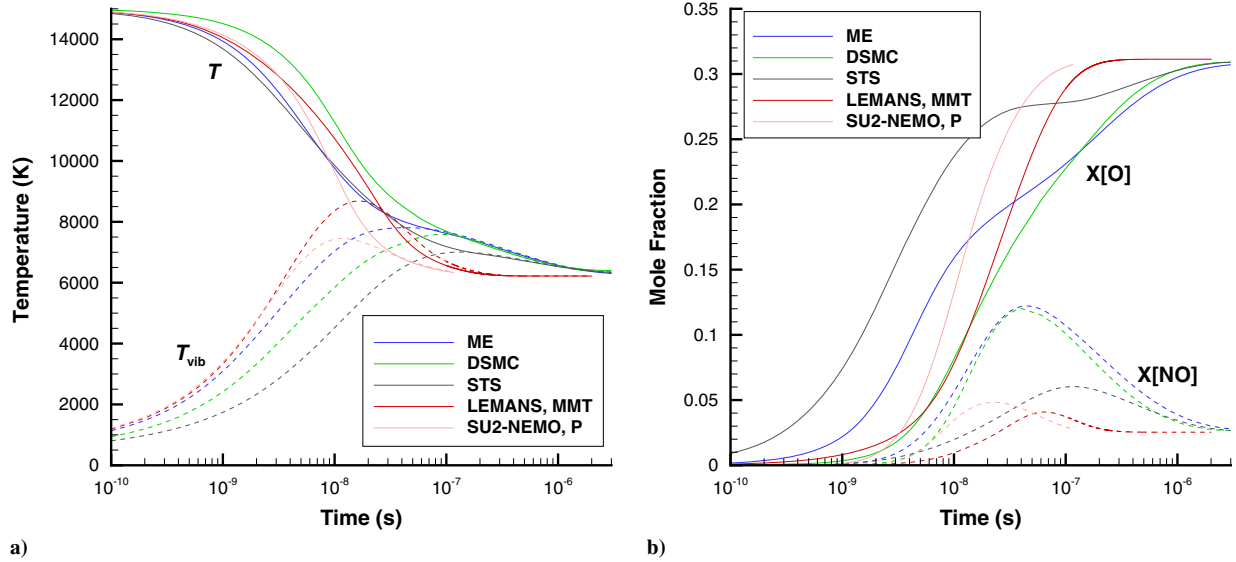


Fig. 14 TC2: temperatures (a) and mole fractions (b) computed with different approaches.

collisions (see Fig. 2b) results in T_{vib} for ME being close to NS. The slowest relaxation of T_{vib} is observed for STS, but T_{trn} decreases quickly for this solver due to fast dissociation. The dissociation is slower in MMT, and especially for DSMC, where strong vibrational favoring is assumed for both oxygen and nitrogen dissociation. Note also very significant differences in maximum T_{vib} , where the highest, MMT, is over 2000 K larger than the lowest, STS. Finally, there are very significant differences in the time to reach steady state, which is over an order of magnitude faster in the NS solvers than in the state-specific solvers. This may be partially attributed to the relatively slow relaxation of populations of high vibrational levels of molecules, both nitrogen and oxygen, which delay the dissociation and thus increases time needed to reach steady state. Interestingly, this effect has not been observed for the lower temperature bath case considered in the previous section, although that case was dominated, at least in the last stage of the relaxation, by the exchange reactions that do not have particularly strong dependence on vibrational populations.

That the agreement between solvers worsens with temperature becomes clear when comparing not only temperatures, but also oxygen and nitric oxide mole fractions, shown in Fig. 14b. There is a qualitative difference between the atomic oxygen mole fractions computed with the fully continuum and state-specific approaches. In the continuum approaches, the mole fraction increases monotonically

from zero to its steady-state value. MMT curve lags behind that of SU2-NEMO, similar to what was observed in Fig. 13b, with that difference being only slightly smaller due to some small differences in the dissociation reaction rate constants. In the state-specific solvers, there is a noticeable change in the slope of $X[\text{O}]$, which is less pronounced in DSMC, but becomes almost a plateau in STS. This, again, is due to the vibration-dissociation coupling, especially that of oxygen: the dissociation reactions deplete primarily higher vibrational levels of molecules, and it takes time to populate them after VVT energy transfer and recombination reactions. There are also some significant differences in the NO mole fractions computed with different solvers. The maximum $X[\text{NO}]$ values are much higher in ME and DSMC than in the other solvers, which is attributed, as will be discussed below, to slow exchange reactions in STS, and very high NO dissociation reaction rates in NS.

As discussed earlier, our primary focus is on species O_2 and NO, both of which may be directly tracked in a shock wave experiment. Similar to the moderate-temperature-bath case considered in the previous section, here we examine the key reaction mechanisms that impact the time dependence of the mole fractions of these species. The contribution of different reactions to the production and the destruction of O_2 and NO computed with DSMC is presented in Fig. 15. The forward and reverse reactions are combined, and the

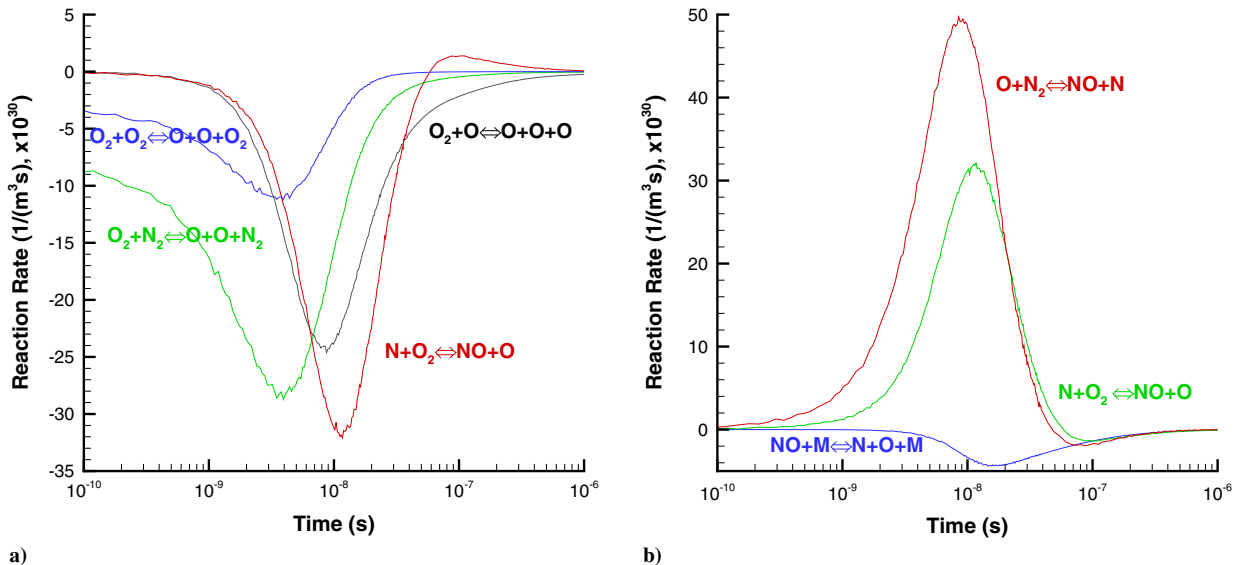


Fig. 15 TC2: contribution of different reaction rates to O_2 (a) and NO (b) density change (DSMC-M2).

processes that result in the decrease and increase of the corresponding mole fractions are plotted in the negative and positive regions of the Y axis. The reactions that at each time moment contribute less than 1% to the total change in the mole fractions are not shown here. Comparing the relative contributions of the dissociation reactions to the lower temperature case shown in Fig. 9, one can see that those are generally similar, with a somewhat larger impact of the $O_2 + O$ dissociation for the 15,000 K case, which may be expected due to significantly higher fraction of O. There is a maximum in the dissociation rate observed as a result of the effect of the increasing vibrational temperature due to VT energy transfer, and decreasing total gas temperature. Interestingly, the contribution of the exchange reaction becomes much more significant than dissociation in the 15,000 K case, which is attributed to the noticeable presence of the atomic nitrogen in the flow. Comparing the impact of the two exchange mechanisms on the NO mole fraction, notice that the $O + N_2$ process is more important until approximately 30 ns, after which time $N + O_2$ has a slightly larger influence on $X[NO]$ (compare this to the lower temperature case, when the contribution from $O + N_2$ was always larger). The dissociation reaction $NO+M$, where M is any of the five air species, plays a minor role.

For the STS approach, again there is a dominance of the $O_2 + N_2$ dissociation reaction (although to a somewhat lesser extent than for the lower temperature case), as illustrated in Fig. 16. Similar to the 7230 K case, there is not maximum in the $N_2 + O_2$ rate, which indicates that even at that temperature the vibration–dissociation coupling is not strong enough for the dependence on the vibrational temperature to be visible. Due to the relatively low rate constant assumed for the $N + O_2$ exchange reaction (see Fig. 4), its impact on $X[O_2]$ is very small for the 15,000 K case. For the NO species, only the $O + N_2$ reaction plays a major role, whereas the contribution of the other exchange reaction, as well as dissociation–recombination process, is less than 10% even at their peak. Compare this to DSMC, where both exchange reactions were found important. Also notice the difference in the location of the peak NO production rate: in DSMC it is close to the peak $X[NO]$, whereas in STS it is observed significantly earlier than the peak $X[NO]$. The lower reaction rates in STS for both exchange reactions as compared to DSMC are responsible for the almost a factor of three difference in the maximum $X[NO]$ obtained in these approaches (see Fig. 14a).

Generally, time-dependent profiles of the dissociation rates are good metrics of the degree of vibrational favoring used in a particular reaction model. Very strong vibrational favoring in DSMC results in very few reactions at the early stages of the relaxation, whereas for a weaker favoring of STS, the dissociation rate decreases with temperature. LeMANS-MMT model is an intermediate case, as illustrated in

Fig. 17a. For the $N_2 + O_2$ oxygen dissociation, the favoring is relatively weak, so that the maximum reaction rate is observed at the beginning of the relaxation. Decreasing gas temperature (translational–rotational) results in decreasing reaction rate afterward. Then, after a few nanoseconds, sharply increased vibrational temperature (see Fig. 14a) reverses that trend, and there is a local peak formed in the reaction rate that roughly corresponds to the peak vibrational temperature. After that, the decrease in all gas temperatures sharply reduces the number of reactions. Similar pattern is observed for the $O_2 + O_2$ reaction, for which the dissociation rate is on average a factor of four lower. Also, the stronger vibrational favoring for this reaction leads to a larger peak in the rate. According to the LeMANS-MMT results, the impact of exchange reactions on $X[O_2]$, although noticeable, is still significantly smaller than that from dissociation. Considering the impact of the exchange reactions on the nitric oxide mole fraction, shown in Fig. 17b, notice that the maximum reaction rate is reached earlier for $O + N_2$ than $N + O_2$. This is due to faster dissociation of oxygen, and thus rapid increase in the number of oxygen atoms in the first 10 ns. This effect, although less pronounced, is also present in DSMC and STS. The $N + O_2$ exchange reaction is somewhat more important than $O + N_2$.

Consider now the impact of reaction channels on gas temperature for different solvers, shown in Fig. 18. According to DSMC, the three most important reactions are oxygen dissociation on N_2 , which dominates the early relaxation stage, followed by the exchange reaction $O + N_2$ and $O + O_2$ dissociation, whose relative importance increases over time. Note also that the exchange reaction proceeds initially mostly in the forward (O_2 destroying), and then, after 30 ns, in the reverse (O_2 producing) direction, which is illustrated by the changing sign of the rate of temperature change for this reaction. The energy contribution from the second exchange reaction, $N + O_2$, is also noticeable, but smaller than from the first, which is related to the 2.5 times smaller energy release after that reaction. There is also some contribution, although relatively small, from nitrogen dissociation. The results obtained with STS solver, qualitatively different from DSMC, indicate that the gas temperature decreases primarily due to the $N_2 + O_2$ oxygen dissociation. Initially, the contribution amounts to over 90% of the total chemical term (the only other visible source being $O_2 + O_2$ dissociation). With the increase of the number of oxygen atoms in the flow, oxygen dissociation on O also becomes a factor, although still not as significant as the $N_2 + O_2$ reaction. The STS rate of temperature change is initially well over an order of magnitude faster than in DSMC due to lower degree of vibrational favoring in dissociation. There is no visible impact of nitrogen dissociation in STS. In the MMT model, the key chemical processes are $N_2 + O_2$ dissociation, $O + NO$ dissociation,

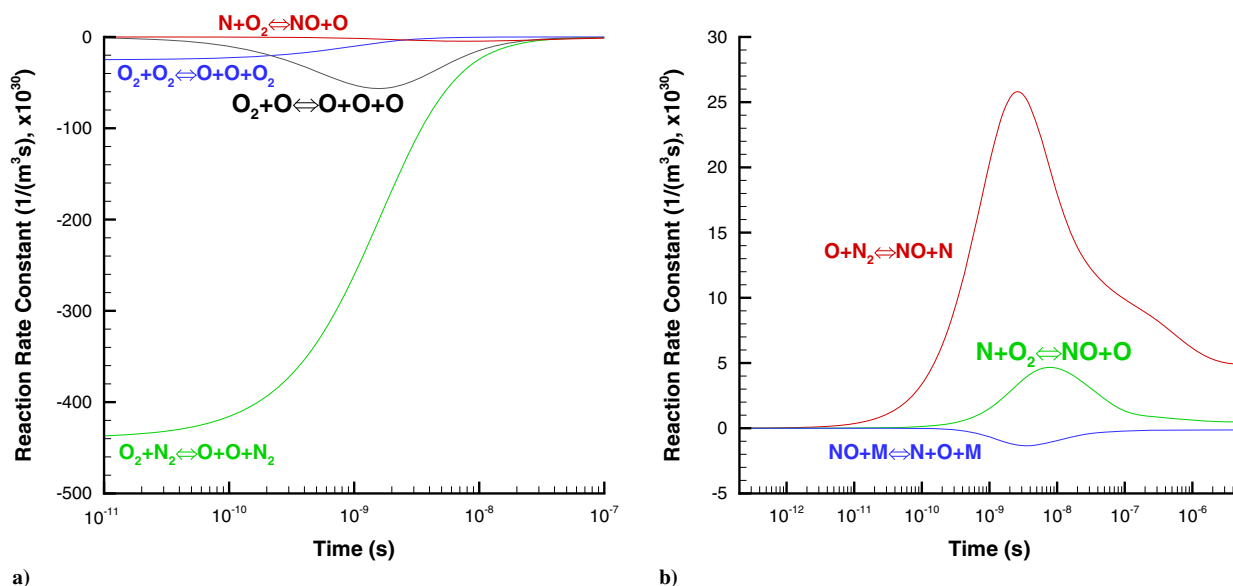


Fig. 16 TC2: contribution of different reaction rates to O_2 (a) and NO (b) density change (STS).

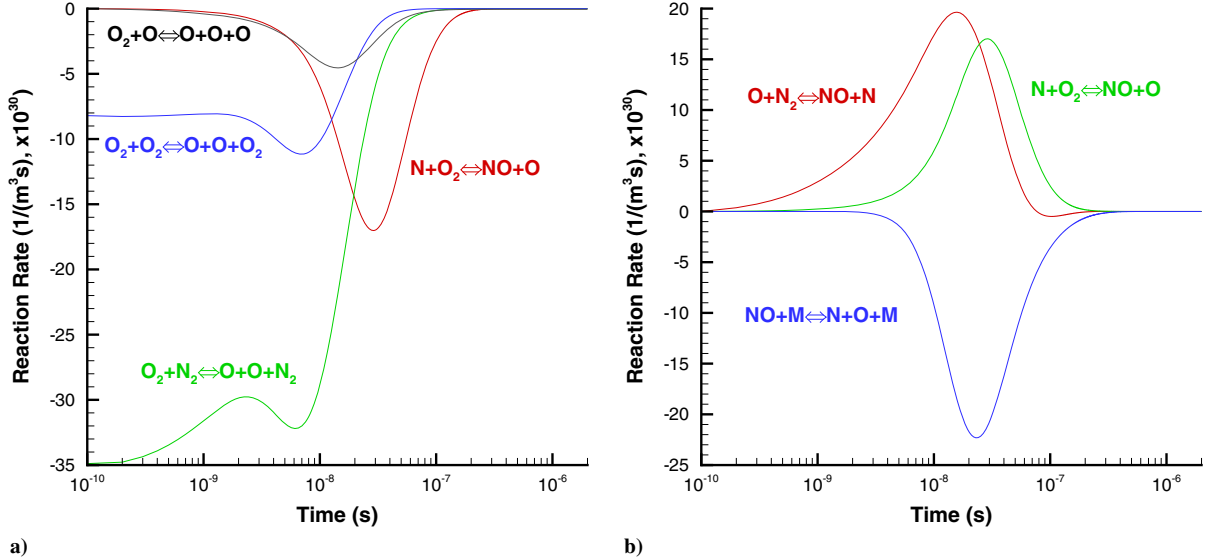


Fig. 17 TC2: contribution of different reaction rates to O_2 (a) and NO (b) density change (LeMANS-MMT).

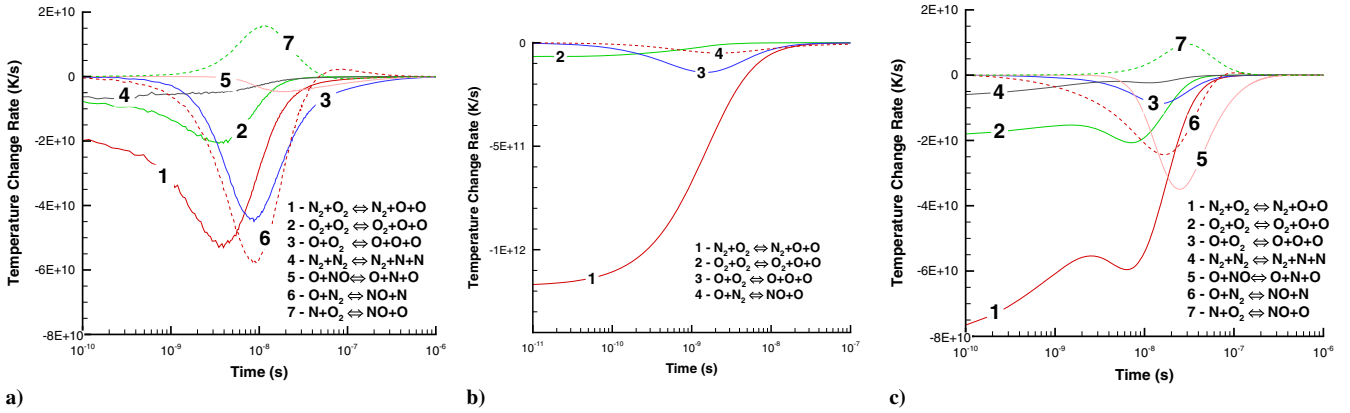


Fig. 18 TC2: impact of reaction channel on the rate of temperature change for DSMC-M2 (a), STS (b), and LeMANS-MMT (c).

and both exchange reactions. The $N_2 + O_2$ dissociation is important approximately the first 20 ns; after that, NO dissociation becomes the largest contributor to the rate. The O_2 dissociation contributions have local maxima at approximately 8 ns due to the increase in vibrational temperature, discussed earlier. This is significantly later than in DSMC, where the maxima were observed at about 3 ns. This difference is due to the single vibrational temperature approximation used in the NS solver: it essentially averages over the vibrational temperature of the fast-relaxing O_2 with the slow-relaxing N_2 . According to MMT, the exchange reactions, and not oxygen dissociation as in DSMC and STS, is the main factor for the decreasing temperature in the later stage of the relaxation (from 20 ns to 1 μ s).

B. Flow over a Cylinder

1. Gas Macroparameters

Of the five solvers used in this work, three are multidimensional and thus can be applied to compute hypersonic flow over a body: the DSMC-based SMILE, and LeMANS and SU2-NEMO that solve NS equations. The gas models used in these solvers to analyze spatially homogeneous relaxation shown earlier are now applied to a 6 km/s air flow over a cylinder, under temperature conditions fairly similar to those of the high-temperature bath case TC2. The peak translational-rotational temperature reaches nearly 15,000 K inside the shock wave at the stagnation streamline; the macroparameters profiles along this line are presented below.

The impact of the DSMC gas model on the overall translational and nitrogen vibrational temperatures is shown in Fig. 19a. These results may be compared to those of Fig. 12, where these models were

applied to the adiabatic heat bath (note that the DSMC-M1 model is not shown in this section as it is fairly close to DSMC-M2). The comparison indicates that the model with the fastest thermal relaxation, DSMC-M4, has the smallest stand-off distance, and vice versa, for DSMC-M2. The primary reason for the noticeable difference in the stand-off distance is the dissociation reaction rates, most importantly, those of N_2 dissociating on N_2 and O . The models DSMC-M2 and DSMC-M3 apply the same reaction rates at equilibrium, but under nonequilibrium conditions, DSMC-M2, which takes into account the effect of vibrational favoring of dissociation, has a lower reaction rate. Initially, it is because the vibrational temperature is much lower than translational, and at a later time, when temperatures nearly equilibrate, it is because of the depletion of high vibrational levels due to the dissociation. DSMC-M3 and DSMC-M4 use the same collision and reaction models, but the dissociation rates are higher in DSMC-M4 (the rate coefficients for DSMC-M3 and DSMC-M4 are reproduced, respectively, by “DSMC” and “LeMANS-Park” in Fig. 3; see also [7]). The stand-off distance is well known to decrease when endothermic reaction rates increase as more energy is transferred from the thermal modes of gas molecules to the potential energy of the created atoms [87]. In all three models, the vibrational temperature is slightly below the translational at the locations between -0.008 and -0.002 m. This is believed to be driven by the endothermic $N_2 + O$ exchange reaction and for DSMC-M2, also by the vibrationally favored dissociation. The peak vibrational temperature largely depends on the dissociation reaction rates, and thus it is lowest for DSMC-M4 and highest for DSMC-M2. Note that there is a visible change of slope near the wall predicted

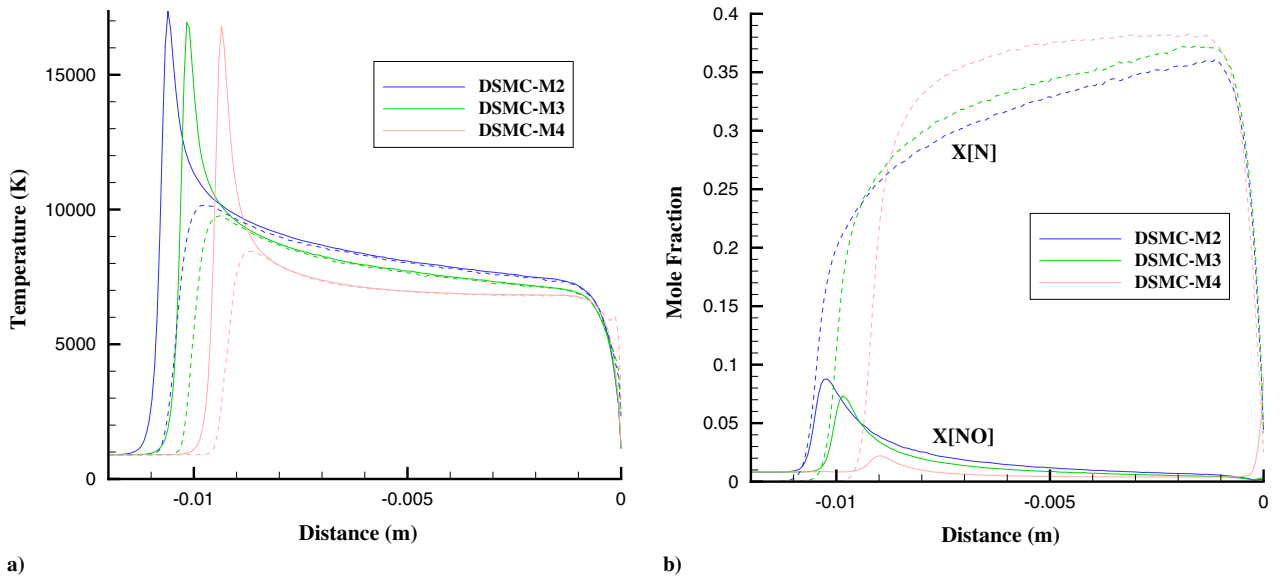


Fig. 19 TC3: impact of the DSMC gas model on translational (solid lines) and N_2 vibrational (dashed lines) temperatures (a) and species mole fractions (b).

with Park's reaction rates, explained by the early offset of the gas-phase recombination of N and O atoms, resulting in the formation of NO and thus a significant heat release into the bulk gas.

The difference in the nonequilibrium reaction rates for the examined DSMC models is clearly manifested in the atomic nitrogen and nitric oxide mole fractions, given in Fig. 19b. For the DSMC-M4 model, $X[N]$ grows rapidly to its quasi-steady-state value of about 0.37. There is a peak of $X[NO]$ observed for this model, but the peak is rather small, approximately 2.3%. For both DSMC-M2 and DSMC-M3, the initially rapid growth in $X[N]$ becomes much more gradual after the first 1 mm into the shock. The reason for the qualitative difference between the DSMC-M2/DSMC-M3 and DSMC-M4 models is the NO dissociation rates. For DSMC-M4, where the NO dissociation rate constants are nearly two orders of magnitude larger, the initial increase is driven by both the fast dissociation of N_2 and NO (the latter is produced in the fast $N_2 + O$ exchange reaction, because the molecular oxygen is almost fully dissociated at that point). For the other two models, the NO dissociation is a minor player, and the increase in $X[N]$ is only due to N_2

dissociation. Moreover, the N_2 dissociation reaction is competing with the $N_2 + O$ exchange, and thus less N is produced. After $X[NO]$ reaches its peak of over 8% for DSMC-M2 and 7% for DSMC-M3, the decreasing gas temperature suppress the highly endothermic $N_2 + O$ exchange process. The reverse exchange reaction becomes more important, in turn increasing the mole fraction of N.

The gas temperatures computed with LeMANS and SU2-NEMO solvers are plotted in Fig. 20a. Both solvers use the preferential Gibbs, Gibbs-P, model, with Park's reaction rate constants; in addition to that, the MMT model is used in LeMANS. Comparing the two reaction models, one can see that the peaks of translational and vibrational temperatures are noticeably, up to 1000 K, higher in MMT. This is generally expected because lower dissociation reaction rates are applied in MMT. There is also small difference between the models in the boundary layer, with MMT temperature also lower. The standoff distance predicted by LeMANS is nearly the same in MMT and Gibbs-P. In SU2-NEMO, which uses the same two-temperature Gibbs-P model, the stand-off distance is about 10% smaller than in LeMANS, and the initial temperature rise is much steeper. The

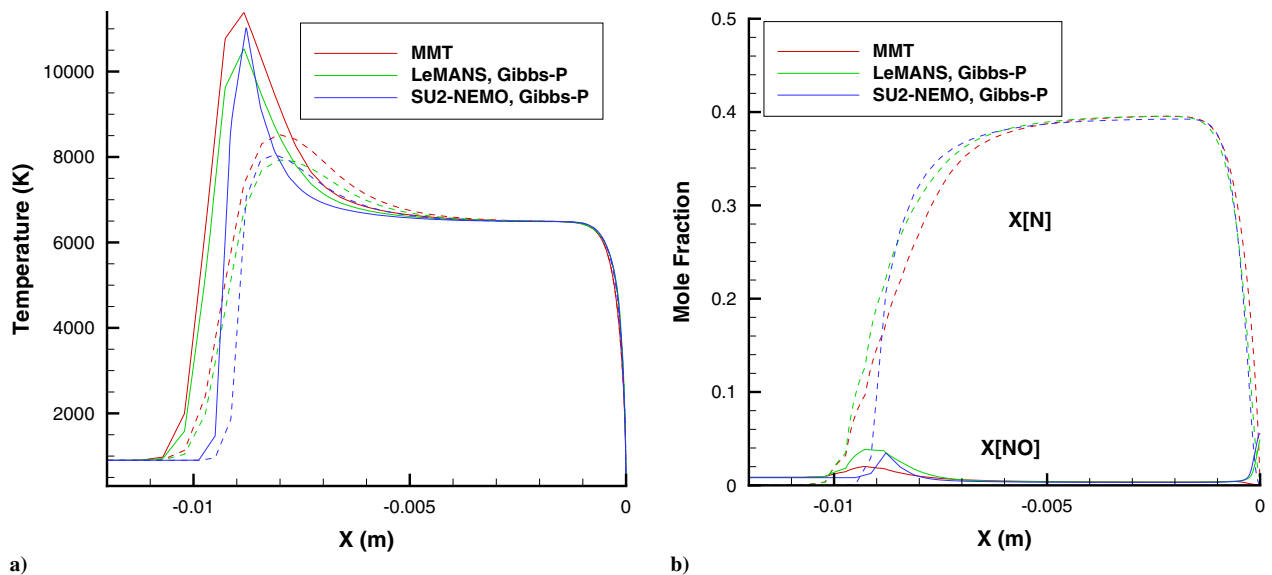


Fig. 20 TC3: impact of the NS solver and reaction model on translational (solid lines) and N_2 vibrational (dashed lines) temperatures (a) and species mole fractions (b).

difference is attributed to differences in the implementation of shock wave discontinuities in these codes, and not to transport or reaction models. Comparing these results with the adiabatic bath, Fig. 13, notice quantitatively similar trend of a higher vibrational peak and slower after-peak relaxation in the MMT model compared to Gibbs-P.

The solver and reaction model effect on the N and NO mole fractions is shown in Fig. 20. Both solvers predict a maximum $X[\text{NO}]$ of less than 4%. This is about 50% larger than that predicted by the DSMC-M4 model, which uses the same Park's reaction rate constants. The difference is attributed primarily to the implementation of the TCE model in the DSMC; even though the model was derived from temperature-dependent reaction rate constants, the reaction probabilities are energy based, and under the conditions of strong thermal nonequilibrium, when the vibrational temperature is much lower than the translational, and vibrational populations are significantly nonequilibrium, the reaction rate in the TCE model will not be equal to that of a continuum approach. The peak $X[\text{NO}]$ in MMT is very close to DSMC-M4. All NS solutions are considerably lower than the peak $X[\text{NO}]$ predicted by DSMC-M2. Note that accurate determination of that peak may be important, with NO being the key flow observable, and experimental data may be necessary to resolve the differences between the models. There are relatively minor differences in $X[\text{NO}]$ obtained by LeMANS and SU2-NEMO, mostly related to the differences in the stand-off distances discussed earlier. Comparing the species mole fraction near the wall, notice the increase of $X[\text{NO}]$ for Park's rates which, similar to the DSMC solution, is due to the fast NO recombination in that region of the flow.

2. Distributed Surface Properties

Consider now the impact of the reaction model on the distributed surface properties over the cylinder. Below, only the distributed heat flux is shown, because the impact of the model and the numerical approach on the distributed pressure and skin friction was found to be within one percent. The distributed heat flux is presented for the DSMC and NS approaches on Figs. 21a and 21b, respectively. Here, the angle of 0 deg corresponds to the stagnation point. In addition to the baseline models, computations were conducted for fully catalytic gas-surface interaction models, in order to approximate the strongly catalytic surface of experiments [3]. In DSMC, the model [53] is used, where all collisions between pairs of atoms in a layer of very small collision cells adjacent to the body are assumed to result in a three-body recombination, with the third partner selected randomly from all particles in that cell. In NS, all nitrogen and oxygen atoms were assumed to react and form molecular nitrogen and oxygen,

respectively. From Fig. 21a it may be concluded that the impact of the nonequilibrium reaction and collision model, cf. DSMC-M2 and DSMC-M3, is negligible, and is essentially within the statistical error bars of the computations. The difference in shock and the aftershock relaxation, including the stand-off distance, therefore has virtually no impact on the surface aerothermodynamics in this case. There is very noticeable, on the order of 10%, impact of the reaction rate constants, cf. DSMC-M3 and DSMC-M4 profiles. Park's rate set predicts a higher heat flux, with the difference for the most part driven by NO recombination (notice also that the relative difference is a weak function of the location along the wall, with the difference at the stagnation point of about 12%, and at 90 deg, less than 8%). The fully catalytic models, as expected, result in further increase of the heat flux due to the exothermic wall recombination. For the DSMC-M2 model, the catalytic processes increase the heat flux at the stagnation point by 25% and at 90 deg, by over a factor of two, although the absolute increase is larger at the stagnation point where more atoms where produced behind the shock due to higher temperatures. Interestingly, there is a visible difference between fully catalytic DSMC-M2 and DSMC-M4 models. This is related to a significant presence of NO in the Knudsen layer around the wall, predicted with Park's reaction rates and discussed earlier, and complemented by a noticeable mole fraction of atomic oxygen. That, in turn, stimulates fast exothermic exchange reaction $\text{NO} + \text{O} \rightarrow \text{O}_2 + \text{N}$, and therefore heat release, as compared to the baseline SMILE rates where NO population near the wall is negligible.

The impact of the reaction rates in the continuum simulations is shown in Fig. 21b, where the QCT-based MMT model is compared with the results based on the Park's reaction rates. The rate effect in NS is similar to DSMC only near the stagnation point, where the Park's model predicts an 11% higher heat flux. At larger angles, the heat flux of the MMT model becomes larger than Park's. Such a crossover is attributed to the nitrogen on oxygen dissociation. Behind the shock, the flow is nearly thermally equilibrium, and thus the reaction rates for this reaction closely follow that shown in Fig. 3a. At higher temperatures, such as those in the coreflow near the stagnation line, the reaction rate constant of the MMT model is higher or close to that recommended by Park. The shock wave at larger distances from the stagnation line is much weaker, and the temperatures, much lower. At those temperatures, the dissociation rate is considerably lower in the MMT model. Lower dissociation rate, and thus lower heat removal from the flow, predictably results in higher heat flux. Catalytic surface significantly increase the heat flux, with the increase for the MMT model fairly similar to that of the baseline DSMC-M2.

Let us now compare the gas and surface properties obtained with NS and DSMC. Figure 22a shows such a comparison for the case

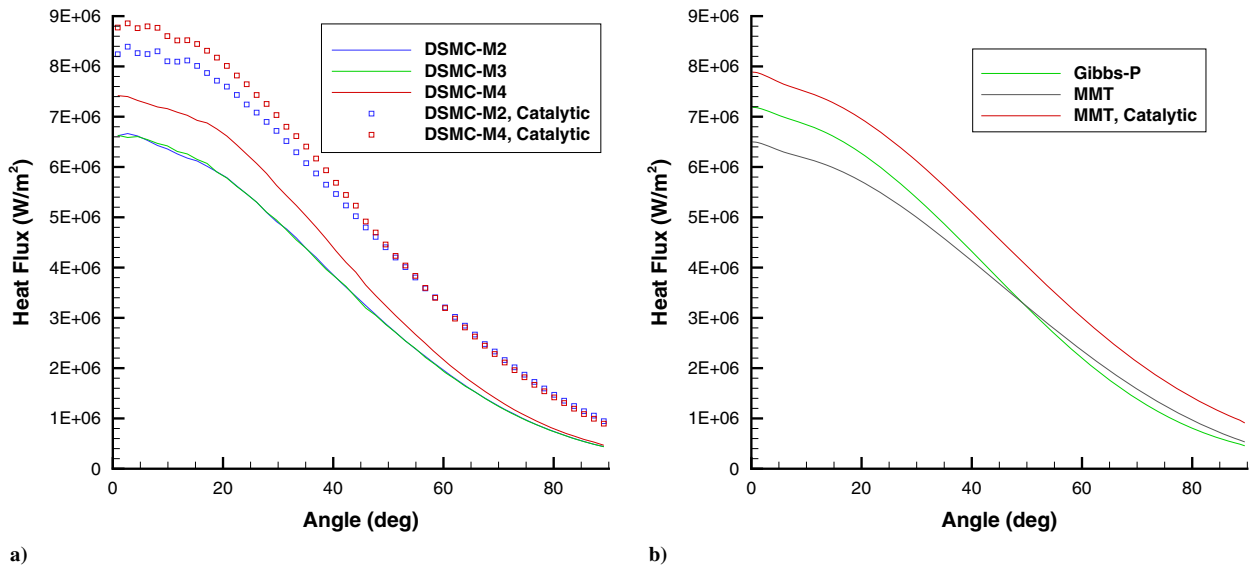


Fig. 21 TC3: distributed surface heat flux obtained by different DSMC (a) and NS (b) models.

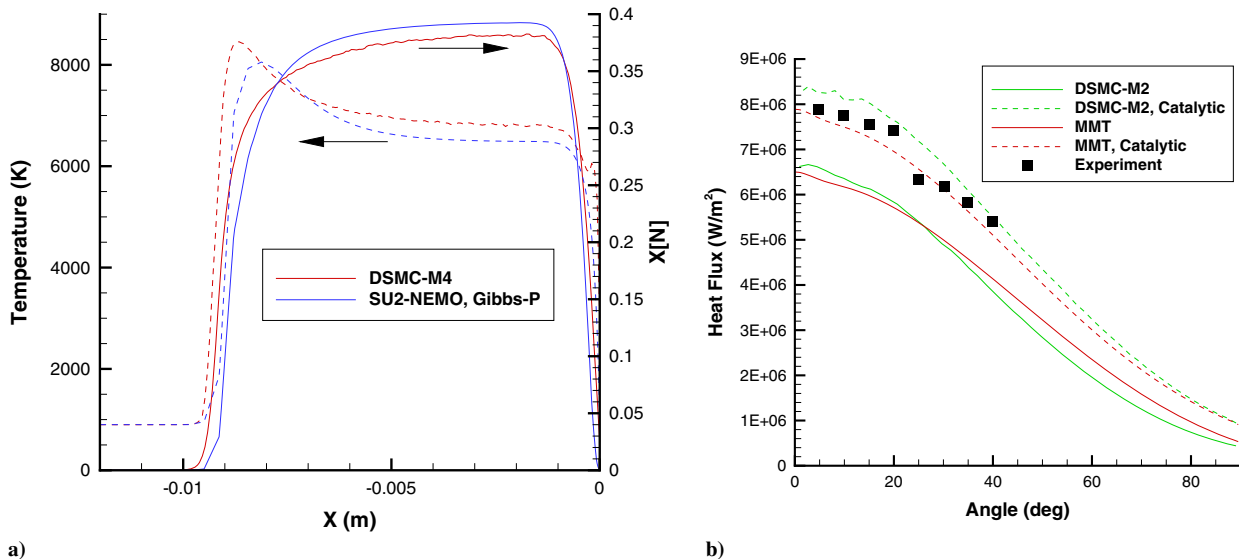


Fig. 22 TC3: comparison of NS and DSMC solutions. Stagnation line properties (a) and distributed heat flux (b).

where the codes use the same reaction rate constants. The gas overall vibrational temperatures and atomic nitrogen mole fractions are shown here. The differences in the standoff distance and peak vibrational temperatures observed in highly nonequilibrium part of the flow are generally expected. For the flow between the shock and the boundary layer, which is close to thermal (but not chemical) equilibrium, implementation details, such as energy modes contributing to reaction rates, and possibly differences in transport properties and vibrational relaxation, are believed to be responsible for somewhat lower degree of dissociation, and thus higher temperature, in DSMC compared to NS. The surface pressure distributions for the DSMC and NS are close, with the DSMC stagnation point value approximately 2% higher, and thus are not shown here. The surface heat fluxes for the high-fidelity DSMC and NS models are given in Fig. 22b, along with the experimental data [3]. Noncatalytic DSMC and NS predictions agree well near the peak value. At larger angles, MMT model predicts visibly higher heat flux. The reason for this is believed to be the same as discussed in the MMT versus Park comparison, namely, the nitrogen dissociation reaction rates (see Fig. 3a). The Bias model of DSMC has the rate constant that is higher than that for MMT at low temperatures, and lower, at high temperatures. The inverse dependence of the heat flux on the dissociation rate causes the observed difference in the slopes for the Bias and MMT models. Interestingly, this difference propagates to the catalytic models, where the slope for the Bias model is also steeper. Both catalytic models reasonably agree with data, with the NS solution being somewhat closer (although it is not clear whether the surface in the experiment was fully catalytic as it was assumed in the computations).

VIII. Discussion

A. Reaction Rates

Large uncertainties in vibrational relaxation and reaction rates for atomic and molecular air species, which are especially significant under conditions of strong thermochemical nonequilibrium, are associated with the lack of accurate and detailed experimental data on these processes. Ideally, each of these processes needs to be evaluated individually in a wide range of flow conditions. In the absence of such data, CFD modelers usually choose rates and models that they believe best reflect the state-of-the-art. Because of this, the five different solvers applied in this work use their standard rates and models as the baseline. Comparison of VT relaxation times assumed or applied in these solvers indicates that for a range of temperatures relevant to hypersonic simulations, there are large, in most cases well over an order of magnitude, uncertainties in collisions that include nitric oxide. There are also an order-of-magnitude differences for the

important $N_2 + O$ interaction. Analysis of the reaction rate constants shows that there is good agreement between all solvers for Zeldovich exchange reactions. Similarly, there is little difference in the assumed equilibrium constants. The largest, up to two orders of magnitude, differences are observed between the NS and the three STS approaches for the dissociation and recombination reactions of NO. The corresponding rate constants of both NS solvers, which are conventionally based on Park's recommendations, systematically overpredict the other three, which are based on recent theoretical predictions.

B. Moderate-Temperature 0D and 1D Relaxation

The moderate temperature adiabatic bath relaxation, where the initial translational-rotational temperature is on the order of 7000 K, is the test case where all solvers and models considered here are used. The computations have clearly shown that there is better agreement in gas temperatures, both translational and vibrational, than in species mole fractions. In the latter, the differences in relaxation time reach an order of magnitude, and the culprit to a large extent was oxygen dissociation on N_2 molecules. For this collision type, more complete and accurate information on vibration-dissociation coupling may be required, applicable to both state-specific and traditional continuum approaches.

Besides 0D heat bath, DSMC computations of a 1D reflected shock wave were also conducted under conditions, where experimental data have recently been obtained on oxygen absorbance under conditions similar to those of the moderate temperature heat bath case. The computations indicate that a reconsideration of the relaxation properties of the currently used VV model may be needed, originally developed based on experimental data obtained at much lower temperatures. The baseline DSMC model was found to capture well the initial rise in absorbance, and the absorbance maximum, but not the sharp decrease after the peak. Comparison of 1D and 0D results indicates that such a decrease may be difficult to capture for all STS approaches considered here. The NS approaches cannot be applied for this comparison as long as they use a two-temperature model; a separation of vibrational temperature by species would be necessary in this case (or in any case where O_2 or NO vibrational temperature or absorbance is measured inside a shock).

C. High-Temperature 0D and 2D Relaxation

The distinctions between solvers significantly increase when the adiabatic bath temperature was increased to 15,000 K. Most notably, there is an over a factor of two difference between the maximum mole fractions of NO. It is much higher in DSMC and the QCT-mole solution of the vibrational kinetic equations than in NS, with the

primary reason being two orders of magnitude higher NO dissociation rates assumed in NS. There are also noticeable differences in the time-dependent profile of atomic oxygen mole fraction, with the state-specific approaches indicating a change of slope related to gas reaching quasi steady state, and dissociation slowing down due to the depopulation of high vibrational levels. The computations allowed the evaluation of separate contributions of different reaction channels to the time evolution of O₂ and NO mole fractions and gas temperature. These contributions were found to be qualitatively different, with the main players being N₂ + O exchange and O₂ + O dissociation in DSMC, O₂ dissociation on N₂ in a vibrational state-specific approach, and NO + O dissociation, in addition to O₂ + N₂ dissociation, in NS.

DSMC simulation of a hypersonic flow over a cylinder shows that, for considered conditions, the nonequilibrium gas model, which includes vibration–dissociation coupling and a high-fidelity treatment of VT energy transfer, has visible impact on the gas properties inside and immediately behind the shock, as well as the shock stand-off distance, but has virtually no effect on the distributed aerothermodynamic properties. Reaction rate constants do impact gas properties and surface heat flux for both DSMC and NS. For the gas properties, the large uncertainties in the dissociation rates of NO have a dominant impact on the peak NO mole fraction. For the heat flux, NO recombination becomes a major player, in addition to nitrogen dissociation. Generally, there is good agreement between NS and DSMC heat fluxes, both for lower-fidelity models based on Park’s reaction rate constants and for higher-fidelity QCT-based models. Peak heat flux for a higher-fidelity model in NS is approximately 10% lower than its lower-fidelity counterpart, with the difference attributed to the dissociation rate constants. NS and DSMC models that include surface catalytic activity agree well with available experimental data on surface heat flux, although this agreement may not be regarded as a comprehensive model validation, for which detailed spectrally and spatially resolved experimental data would be necessary.

D. Code-to-Code Differences

In the ideal case of fully defined and consistent physical and chemical models applied in different CFD solvers, with matching rates and compatible models, differences in the results would be negligible. This is often not the case, though, as the results are also influenced by various numerical parameters. An example of this effect was shown in this work, where the application of two NS solvers with identical physical models resulted in virtually identical results in adiabatic baths, but visibly different stand-off distances for a hypersonic flow over a cylinder.

E. Effect of Vibrational Relaxation and Reaction Model

Multiple comparisons presented in this work illustrate how the uncertainties in relaxation and reaction rates are exacerbated by uncertainties related to nonequilibrium collision and reaction models. In NS solvers, changing nonpreferential to preferential model of vibrational energy lost to dissociation has visible, but still relatively small, impact on gas relaxation. However, replacing the conventional 2D-Park reaction model with MMT has large effect on both overall and species properties, where the MMT relaxation is several times slower than 2T-Park. Similarly, in DSMC, the vibrationally favored Bias dissociation model results in much slower relaxation than the conventional TCE model, and this model effect is sometimes larger than the effect of the rates. While it is tempting to conclude that the Bias model in DSMC and the MMT model in NS better capture the properties of real reacting air than their simpler conventional counterpart, as they certainly offer improved physical realism, certain caution needs to be used before such a conclusion is drawn. The reason being the lack of detailed parametric validation of these models with accurate and time-resolved experimental data in a sufficiently wide range of temperatures.

F. Validation: What Is Missing?

With the impressive progress achieved over the last decade at shock tube facilities, where time-accurate emission and absorption

diagnostics were applied behind incident shock waves (NASA EAST and Moscow State facilities) and, most recently, reflected shock waves (Stanford reflected shock facility) at highly nonequilibrium, hypersonic conditions, the daunting task of nonequilibrium high-temperature air model validation may finally be within reach. For validation efforts to be successful, time-resolved diagnostics with error bars within 5% would be highly desirable, in the range of temperatures from 5000 to 15,000 K. In this work, several aspects that would be useful for such a validation are highlighted,

- 1) Nitric oxide relaxation and dissociation properties
- 2) VT energy transfer in collisions of atoms with N₂, as well as N₂ dissociation rate
- 3) Peak nitric oxide mole fraction behind strong shock waves
- 4) Vibrational favoring of N₂, O₂, and NO dissociation
- 5) Reaction paths most important in moderate- and high-temperature regimes.

IX. Conclusions

Five gas flow solvers that use fully kinetic, vibrationally kinetic, and continuum approaches are applied to model high temperature thermal and chemical relaxation of air in an adiabatic heat bath and a hypersonic flow over a cylinder. Significant uncertainties in vibration-translation relaxation time and dissociation, recombination, and exchange reaction rates are shown to have a profound effect on gas temperature and species mole fractions. Accurate experimental data are required to reduce these uncertainties, especially in collisions that include nitric oxide.

Acknowledgments

The work at Air Force Research Laboratory was supported by the Air Force Office of Scientific Research (Program Officers Ivett Leyva and Sarah Popkin). The work of Olga V. Kunova and Elena V. Kustova was supported by Saint Petersburg State University, Project ID 84912260. Sergey F. Gimelshein and Ingrid J. Wysong are grateful to Jesse Streicher and Ron Hanson for many fruitful discussions of reflected shock experiments and simulations, and for the information on the flow conditions of the reflected shock experiments. Kyle M. Hanquist also thanks Ross Chaudhry for several useful discussions on the Modified Marrone–Treanor model, and Martin Liza for processing the LeMANS data.

References

- [1] Holloway, M. E., Hanquist, K. M., and Boyd, I. D., “Assessment of Thermochemistry Modeling for Hypersonic Flow over a Double Cone,” *Journal of Thermophysics and Heat Transfer*, Vol. 34, No. 3, 2020, pp. 1–10.
<https://doi.org/10.2514/1.T5792>
- [2] Hornung, H., and Leyva, I., “Sonic Line and Shock Detachment in Hypervelocity Cone Flow,” *IUTAM Symposium Transsonicum IV, Fluid Mechanics and Its Application*, Vol. 73, edited by H. Sobieczky, Springer, Dordrecht, Germany, 2003, pp. 381–386.
https://doi.org/10.1007/978-94-010-0017-8_56
- [3] Karl, S., Martinez-Schramm, J., and Hannemann, K., “High Enthalpy Cylinder Flow in HEG: A Basis for CFD Validation,” *AIAA Paper 2003-4252*, 2003.
<https://doi.org/10.2514/6.2003-4252>
- [4] Holden, M., MacLean, M., Wadhams, T., and Dufrene, A., “Measurements of Real Gas Effects on Regions of Laminar Shock Wave/Boundary Layer Interaction in Hypervelocity Flows for Blind Code Validation Studies,” *AIAA Paper 2013-2837*, 2013.
- [5] Ibraguimova, L., Sergievskaya, A., Levashov, V., Shatalov, O., Tunik, Y., and Zabelinskii, I., “Investigation of Oxygen Dissociation and Vibrational Relaxation at Temperatures 4000–10800 K,” *Journal of Chemical Physics*, Vol. 139, No. 3, 2013, Paper 034317.
<https://doi.org/10.1063/1.4813070>
- [6] Candler, G., “Rate Effects in Hypersonic Flows,” *Annual Review of Fluid Mechanics*, Vol. 51, Jan. 2019, pp. 379–402.
<https://doi.org/10.1146/annurev-fluid-010518-040258>
- [7] Gimelshein, S., Wysong, I., Fangman, A., Andrienko, D., Kunova, O., Kustova, E., Garbacz, C., Fossati, M., and Hanquist, K., “Kinetic and Continuum Modeling of High Temperature Relaxation of O₂ and N₂

- Binary Mixtures,” *Journal of Thermophysics and Heat Transfer*, 2022. <https://doi.org/10.2514/1.T6258>
- [8] Cortesi, A., Constantine, P., Magin, T., and Congedo, P., “Forward and Backward Uncertainty Quantification with Active Subspaces: Application to hypersonic Flows Around a Cylinder,” INRIA Research Rept. 9097, Paris, 2017, pp. 1–41.
- [9] Ray, J., Kieweg, S., Dinzi, D., Carnes, B., Weirs, V., Freno, B., Howard, M., Smith, T., Nompelis, I., and Candler, G. V., “Estimation of Inflow Uncertainties in Laminar Hypersonic Double-Cone Experiments,” *AIAA Journal*, Vol. 58, No. 10, 2020, pp. 4461–4474. <https://doi.org/10.2514/6.2019-2279>
- [10] Li, Z., Parsons, N., and Levin, D., “A Study of Internal Energy Relaxation in Shocks Using Molecular Dynamics Based Models,” *Journal of Chemical Physics*, Vol. 143, No. 145, 2015, Paper 144501. <https://doi.org/10.1063/1.4931107>
- [11] Luo, H., Kulakhmetov, M., and Alexeenko, A., “Ab Initio State-Specific $N_2 + O$ Dissociation and Exchange Modeling for Molecular Simulations,” *Journal of Chemical Physics*, Vol. 146, No. 7, 2017, Paper 074303. <https://doi.org/10.1063/1.4975770>
- [12] Streicher, J., Krish, A., and Hanson, R., “Shock-Tube Measurements of Vibrational Relaxation Times in Oxygen and Nitrogen Mixtures Using Ultraviolet Laser Absorption Spectroscopy,” AIAA Paper 2020-1940, 2020. <https://doi.org/10.2514/6.2020-1940>
- [13] Hanquist, K., Chaudhry, R., Boyd, I., Streicher, J., Krish, A., and Hanson, R., “Detailed Thermochemical Modeling of O_2 -Ar in Reflected Shock Tube Flows,” AIAA Paper 2020-3275, 2020. <https://doi.org/10.2514/6.2020-3275>
- [14] Streicher, J., Krish, A., and Hanson, R., “Vibrational Relaxation Time Measurements in Shock-Heated Oxygen and Air from 2000 K to 9000 K Using Ultraviolet Laser Absorption,” *Physics of Fluids*, Vol. 32, No. 8, 2020, Paper 086101. <https://doi.org/10.1063/5.0015890>
- [15] Streicher, J. W., Krish, A., Hanson, R. K., Hanquist, K. M., Chaudhry, R. S., and Boyd, I. D., “Shock-Tube Measurements of Coupled Vibration-Dissociation Time-Histories and Rate Parameters in Oxygen and Argon Mixtures from 5,000-10,000 K,” *Physics of Fluids*, Vol. 32, No. 7, 2020, Paper 076103. <https://doi.org/10.1063/5.0012426>
- [16] McGilvray, M., Doherty, L., Morgan, R., and Gildfind, D., “T6: The Oxford University Stalker Tunnel,” AIAA Paper 2015-3545, 2015. <https://doi.org/10.2514/6.2015-3545>
- [17] Leibowitz, M., “Hypervelocity Shock Tunnel Studies of Blunt Body Aerothermodynamics in Carbon Dioxide for Mars Entry,” Ph.D. Thesis, California Inst. of Technology, Pasadena, CA, 2020. <https://doi.org/10.7907/chyn-ea06>
- [18] Gimelshein, S., and Wysong, I., “Hypersonic Non-Equilibrium Comparison Cases,” *AIP Conference Proceedings*, Vol. 2132, No. 1, 2019, Paper 100008. <https://doi.org/10.1063/1.5119603>
- [19] Olthoff, J., and Greenberg, K., “The Gaseous Electronics Conference RF Reference Cell—An Introduction,” *Journal of Research of the National Institute of Standards and Technology*, Vol. 100, No. 4, 1995, p. 327.
- [20] Gimelshein, S., “Particle Modeling of Reflected Shock Waves,” *Journal of Thermophysics and Heat Transfer*, Vol. 35, No. 2, 2021, pp. 362–371. <https://doi.org/10.2514/1.T6103>
- [21] Gimelshein, S., and Wysong, I., “Nonequilibrium Air Flow Predictions with a High-Fidelity Direct Simulation Monte Carlo Approach,” *Physical Review Fluids*, Vol. 4, No. 3, 2019, Paper 033405. <https://doi.org/10.1103/PhysRevFluids.4.033405>
- [22] Ivanov, M., Markelov, G., and Gimelshein, S., “Statistical Simulation of the Transition Between Regular and Mach Reflection in Steady Flows,” *Computers and Mathematics with Applications*, Vol. 35, Nos. 1–2, 1998, pp. 113–126. [https://doi.org/10.1016/S0898-1221\(97\)00262-9](https://doi.org/10.1016/S0898-1221(97)00262-9)
- [23] Adamovich, I., “Three-Dimensional Analytic Model of Vibrational Energy Transfer in Molecule-Molecule Collisions,” *AIAA Journal*, Vol. 39, No. 10, 2001, pp. 1916–1925. <https://doi.org/10.2514/2.1181>
- [24] Andrienko, D. A., and Boyd, I. D., “Rovibrational Energy Transfer and Dissociation in O_2 -O Collisions,” *Journal of Chemical Physics*, Vol. 144, No. 10, 2016, Paper 104301. <https://doi.org/10.1063/1.4943114>
- [25] Paukku, Y., Varga, Z., and Truhlar, D. G., “Potential Energy Surface of Triplet O_4 ,” *Journal of Chemical Physics*, Vol. 148, No. 12, 2018, Paper 124314. <https://doi.org/10.1063/1.5017489>
- [26] Varga, Z., Paukku, Y., and Truhlar, D. G., “Potential Energy Surfaces for $O + O_2$ Collisions,” *Journal of Chemical Physics*, Vol. 147, No. 15, 2017, Paper 154312. <https://doi.org/10.1063/1.4997169>
- [27] Jaffe, R., Schwenke, D., Chaban, G., and Huo, W., “Vibrational and Rotational Excitation and Relaxation of Nitrogen from Accurate Theoretical Calculations,” AIAA Paper 2008-1208, 2008. <https://doi.org/10.2514/6.2008-1208>
- [28] Bender, J. D., Valentini, P., Nompelis, I., Paukku, Y., Varga, Z., Truhlar, D. G., Schwartztruber, T., and Candler, G. V., “An Improved Potential Energy Surface and Multi-Temperature Quasiclassical Trajectory Calculations of $N_2 + N_2$ Dissociation Reactions,” *Journal of Chemical Physics*, Vol. 143, No. 5, 2015, Paper 054304. <https://doi.org/10.1063/1.4927571>
- [29] Campoli, L., Kunova, O., Kustova, E., and Melnik, M., “Models Validation and Code Profiling in State-to-State Simulations of Shock Heated Air Flows,” *Acta Astronautica*, Vol. 175, Oct. 2020, pp. 493–509. <https://doi.org/10.1016/j.actaastro.2020.06.008>
- [30] Adamovich, I., Macheret, S., Rich, J., and Treanor, C., “Vibrational Energy Transfer Rates Using a Forced Harmonic Oscillator Model,” *Journal of Thermophysics and Heat Transfer*, Vol. 12, 1998, pp. 57–65. <https://doi.org/10.2514/2.6302>
- [31] Oblapenko, G., “Calculation of Vibrational Relaxation Times Using a Kinetic Theory Approach,” *Journal of Physical Chemistry A*, Vol. 122, No. 50, 2018, pp. 9615–9625. <https://doi.org/10.1021/acs.jpca.8b09897>
- [32] Kustova, E., and Savelev, A., “Generalized Model for State-Resolved Chemical Reaction Rate Coefficients in High-Temperature Air,” *Journal of Physics: Conference Series*, Vol. 1959, July 2021, Paper 012033. <https://doi.org/10.1088/1742-6596/1959/1/012033>
- [33] Economon, T. D., Palacios, F., Copeland, S. R., Lukaczyk, T. W., and Alonso, J. J., “SU2: An Open-Source Suite for Multiphysics Simulation and Design,” *AIAA Journal*, Vol. 54, No. 3, 2016, pp. 828–846. <https://doi.org/10.2514/1.J053813>
- [34] Millikan, R., and White, D., “Systematics of Vibrational Relaxation,” *Journal of Chemical Physics*, Vol. 39, No. 12, 1963, pp. 3209–3213. <https://doi.org/10.1063/1.1734182>
- [35] Park, C., “Review of Chemical-Kinetic Problems of Future NASA Missions. I—Earth Entries,” *Journal of Thermophysics and Heat Transfer*, Vol. 7, No. 3, 1993, pp. 385–398. <https://doi.org/10.2514/3.431>
- [36] Park, C., “Assessment of Two-Temperature Kinetic Model for Ionizing Air,” *Journal of Thermophysics and Heat Transfer*, Vol. 3, No. 3, 1989, pp. 233–244. <https://doi.org/10.2514/3.28771>
- [37] Park, C., Jaffe, R. L., and Partridge, H., “Chemical-Kinetic Parameters of Hyperbolic Earth Entry,” *Journal of Thermophysics and Heat Transfer*, Vol. 15, No. 1, 2001, pp. 76–90. <https://doi.org/10.2514/2.6582>
- [38] Scalabrin, L. C., “Numerical Simulation of Weakly Ionized Hypersonic Flow over Reentry Capsules,” Ph.D. Thesis, Univ. of Michigan, Ann Arbor, MI, 2007.
- [39] Chaudhry, R. S., and Candler, G. V., “Statistical Analyses of Quasiclassical Trajectory Data for Air Dissociation,” *AIAA Scitech 2019 Forum*, AIAA Paper 2019-0789, 2019. <https://doi.org/10.2514/6.2019-0789>
- [40] Bird, G. A., *Molecular Gas Dynamics and the Direct Simulation of Gas Flows*, Clarendon Press, Oxford, 1994, Chap. 10.
- [41] Bird, G., “Monte Carlo Simulations in an Engineering Context,” *Progress in Astronautics and Aeronautics*, Vol. 74, Jan. 1981, pp. 239–255. <https://doi.org/10.2514/5.9781600865480.0239.0255>
- [42] Capetelli, M., Gorse, C., Longo, S., and Giordano, D., “Collision Integrals of High-Temperature Air Species,” *Journal of Thermophysics and Heat Transfer*, Vol. 14, No. 2, 2000, pp. 259–268. <https://doi.org/10.2514/2.6517>
- [43] Borgnakke, C., and Larsen, P., “Statistical Collision Model for Monte Carlo Simulation of Polyatomic Gas Mixture,” *Journal of Computational Physics*, Vol. 18, No. 4, 1975, pp. 405–420. [https://doi.org/10.1016/0021-9991\(75\)90094-7](https://doi.org/10.1016/0021-9991(75)90094-7)
- [44] Gimelshein, S., Boyd, I., and Ivanov, M., “DSMC Modeling of Vibration-Translation Energy Transfer in Hypersonic Rarefied Flows,” AIAA Paper 1999-3451, June 1999. <https://doi.org/10.2514/6.1999-3451>
- [45] Liechty, D., and Lewis, M., “Treatment of Electronic Energy Level Transition and Ionization Following the Particle-Based Chemistry

- Model,” AIAA Paper 2010-0449, 2010.
<https://doi.org/10.2514/6.2010-449>
- [46] Gimelshein, S., Wysong, I., and Adamovich, I., “Application of the 3D Forced Harmonic Oscillator Model in the DSMC Method,” *Journal of Thermophysics and Heat Transfer*, Vol. 32, No. 4, 2018, pp. 882–891.
<https://doi.org/10.2514/1.T5228>
- [47] Bergemann, F., and Boyd, I., “DSMC Simulation of Inelastic Collisions Using the Borgnakke-Larsen Method Extended to Discrete Distributions of Vibrational Energy,” *Rarefied Gas Dynamics: Theory and Simulations*, edited by B. D. Shizgal, and D. P. Weaver, Vol. 32, Progress in Astronautics and Aeronautics, AIAA, Washington, D.C., 1996, pp. 174–183.
- [48] Kulakhmetov, M., Gallis, M., and Alexeenko, A., “Ab Initio-Informed Maximum Entropy Modeling of Rovibrational Relaxation and State-Specific Dissociation with Application to the $O_2 + O$ System,” *Journal of Chemical Physics*, Vol. 144, No. 17, 2016, Paper 174302.
<https://doi.org/10.1063/1.4947590>
- [49] Gimelshein, N., Gimelshein, S., and Levin, D., “Vibrational Relaxation Rates in the Direct Simulation Monte Carlo Method,” *Physics of Fluids*, Vol. 14, No. 12, 2002, pp. 4452–4455.
<https://doi.org/10.1063/1.1517297>
- [50] Gimelshein, S., and Wysong, I., “Modeling of Vibration-Vibration Energy Transfer in the DSMC Method,” *Journal of Thermophysics and Heat Transfer*, Vol. 32, No. 31, 2018, pp. 781–788.
<https://doi.org/10.2514/1.T5331>
- [51] Koura, K., “A Set of Model Cross Sections for the Monte Carlo Simulation of Rarefied Real Gases: Atom-Diatom Collisions,” *Physics of Fluids*, Vol. 6, No. 10, 1994, pp. 3473–3486.
<https://doi.org/10.1063/1.868404>
- [52] Wadsworth, D., and Wysong, I., “Vibrational Favoring Effect in DSMC Dissociation Models,” *Physics of Fluids*, Vol. 9, No. 12, 1997, pp. 3873–3884.
<https://doi.org/10.1063/1.869487>
- [53] Gimelshein, S., and Wysong, I., “DSMC Modeling of Flows with Recombination Reactions,” *Physics of Fluids*, Vol. 29, No. 6, 2017, Paper 067106.
<https://doi.org/10.1063/1.49865297>
- [54] Park, C., “Problems of Rate Chemistry in the Flight Regimes of Aero-assisted Orbital Transfer Vehicles,” *Progress in Astronautics and Aeronautics*, Vol. 6, June 1985, pp. 511–537.
<https://doi.org/10.2514/6.1984-1730>
- [55] Park, C., *Nonequilibrium Hypersonic Aerothermodynamics*, Wiley, New York, 1990, Chap. 8.
- [56] McBride, B., Zehe, M., and Gordon, S., “NASA Glenn Coefficients for Calculating Thermodynamic Properties of Individual Species,” NASA TP 2002-211556, 2002.
- [57] Andrienko, D. A., and Boyd, I. D., “Thermal Relaxation of Molecular Oxygen in Collisions with Nitrogen Atoms,” *Journal of Chemical Physics*, Vol. 145, No. 1, 2016, Paper 014309.
<https://doi.org/10.1063/1.4955199>
- [58] Andrienko, D., and Boyd, I. D., “State-Resolved Characterization of Nitric Oxide Formation in Shock Flows,” AIAA Paper 2018-1233, 2018.
<https://doi.org/10.2514/6.2018-1233>
- [59] Chaudhry, R., Grover, M., Bender, J., Schwartzentruber, T., and Candler, G., “Quasiclassical Trajectory Analysis of Oxygen Dissociation via O_2 , O, and N_2 ,” AIAA Paper 2018-0237, 2018.
<https://doi.org/10.2514/6.2018-0237>
- [60] Nagnibeda, E., and Kustova, E., *Nonequilibrium Reacting Gas Flows. Kinetic Theory of Transport and Relaxation Processes*, Springer-Verlag, Berlin, 2009, Chap. 1.
<https://doi.org/10.1007/978-3-642-01390-4>
- [61] Kustova, E., “On the Simplified State-to-State Transport Coefficients,” *Chemical Physics*, Vol. 270, No. 1, 2001, pp. 177–195.
[https://doi.org/10.1016/S0301-0104\(01\)00352-4](https://doi.org/10.1016/S0301-0104(01)00352-4)
- [62] Kunova, O., Kustova, E., Mekhonoshina, M., and Nagnibeda, E., “Nonequilibrium Kinetics, Diffusion and Heat Transfer in Shock Heated Flows of N_2/N and O_2/O Mixtures,” *Chemical Physics*, Vol. 463, Dec. 2015, pp. 70–81.
<https://doi.org/10.1016/j.chemphys.2015.10.004>
- [63] Marrone, P., and Treanor, C., “Chemical Relaxation with Preferential Dissociation from Excited Vibrational Levels,” *Physics of Fluids*, Vol. 6, No. 9, 1963, pp. 1215–1221.
<https://doi.org/10.1063/1.1706888>
- [64] Aliat, A., “State-to-State Dissociation-Recombination and Chemical Exchange Rate Coefficients in Excited Diatomic Gas Flows,” *Physica A: Statistical Mechanics and Its Applications*, Vol. 387, Nos. 16–17, 2008, pp. 4163–4182.
<https://doi.org/10.1016/j.physa.2008.02.004>
- [65] Kunova, O., Kustova, E., and Savelev, A., “Generalized Treanor–Marrone Model for State-Specific Dissociation Rate Coefficients,” *Chemical Physics Letters*, Vol. 659, Aug. 2016, pp. 80–87.
<https://doi.org/10.1016/j.cplett.2016.07.006>
- [66] Kustova, E., Savelev, A., and Kunova, O., “Rate Coefficients of Exchange Reactions Accounting for Vibrational Excitation of Reagents and Products,” *AIP Conference Proceedings*, Vol. 1959, 2018, Paper 060010.
<https://doi.org/10.1063/1.5034671>
- [67] Martin, A., Scalabrin, L. C., and Boyd, I. D., “High Performance Modeling of Atmospheric Re-Entry Vehicles,” *Journal of Physics: Conference Series*, Vol. 341, 2012, pp. 1–12.
<https://doi.org/10.1088/1742-6596/341/1/012002>
- [68] Scoggins, J. B., Leroy, V., Bellas-Chatzigeorgis, G., Dias, B., and Magin, T. E., “Mutation++: Multicomponent Thermodynamic and Transport Properties for Ionized Gases in C++,” *SoftwareX*, Vol. 12, July–Dec. 2020, Paper 100575.
<https://doi.org/10.1016/j.softx.2020.100575>
- [69] Liou, M.-S., and Steffen, C. J., “A New Flux Splitting Scheme,” *Journal of Computational Physics*, Vol. 107, No. 1, 1993, pp. 23–39.
<https://doi.org/10.1006/jcph.1993.1122>
- [70] MacCormack, R. W., and Candler, G. V., “The Solution of the Navier-Stokes Equations Using Gauss-Seidel Line Relaxation,” *Computers & Fluids*, Vol. 17, No. 1, 1989, pp. 135–150.
[https://doi.org/10.1016/0045-7930\(89\)90012-1](https://doi.org/10.1016/0045-7930(89)90012-1)
- [71] Landau, L., and Teller, E., “Theory of Sound Dispersion,” *Physik Zeitschrift der Sowjetunion*, Vol. 10, Sept. 1936, pp. 34–38.
- [72] Candler, G. V., and MacCormack, R. W., “Computation of Weakly Ionized Hypersonic Flows in Thermochemical Nonequilibrium,” *Journal of Thermophysics and Heat Transfer*, Vol. 5, No. 3, 1991, pp. 266–273.
<https://doi.org/10.2514/3.260>
- [73] Scoggins, J. B., “Development of Numerical Methods and Study of Coupled Flow, Radiation, and Ablation Phenomena for Atmospheric Entry,” Ph.D. Thesis, von Karman Inst. for Fluid Dynamics, Sint-Genesius-Rode, Belgium, 2017.
- [74] Lee, J.-H., “Basic Governing Equations for the Flight Regimes of Aeroassisted Orbital Transfer Vehicles,” *19th AIAA Thermophysics Conference*, AIAA Paper 1984-1729, 1984, pp. 1–18.
<https://doi.org/10.2514/6.1984-1729>
- [75] Gurvich, L. V., Veits, I. V., and Alcock, C. B., Thermodynamics Properties of Individual Substances, Vol. 1—Elements O, H/D, T, F, Cl, Br, I, He, Ne, Ar, Kr, Xe, Rn, S, N, P, and their Compounds. Part 1—Methods and Computation, 4th ed., Hemisphere Publishing Corp., New York, 1989, Chaps. 4, 13.
- [76] Gurvich, L. V., Veits, I. V., and Alcock, C. B., Thermodynamics Properties of Individual Substances, Vol. 1—Elements O, H/D, T, F, Cl, Br, I, He, Ne, Ar, Kr, Xe, Rn, S, N, P, and their Compounds. Part 2—Methods and Computation, 4th ed., Hemisphere Publishing Corp., New York, 1989, pp. 3, 9, 194, 198, 203.
- [77] Chaudhry, R. S., Boyd, I. D., Torres, E., Schwartzentruber, T. E., and Candler, G., “Implementation of a Chemical Kinetics Model for Hypersonic Flows in Air for High-Performance CFD,” *AIAA Scitech 2020 Forum*, AIAA Paper 2020-2191, 2020.
<https://doi.org/10.2514/6.2020-2191>
- [78] Marrone, P. V., and Treanor, C. E., “Chemical Relaxation with Preferential Dissociation from Excited Vibrational Levels,” *Physics of Fluids*, Vol. 6, No. 9, 1963, pp. 1215–1221.
<https://doi.org/10.1063/1.1706888>
- [79] Park, C., “Review of Chemical-Kinetic Problems of Future NASA Missions, I: Earth Entries,” *Journal of Thermophysics and Heat Transfer*, Vol. 7, No. 2, 1993, pp. 385–398.
<https://doi.org/10.2514/3.431>
- [80] McNeal, R., Whitson, M., and Cook, J., “Temperature Dependence of the Quenching of Vibrationally Excited Nitrogen by Atomic Oxygen,” *Journal of Geophysical Research*, Vol. 79, No. 10, 1974, pp. 1527–1531.
<https://doi.org/10.1063/1.434217>
- [81] Wray, K., “Shock-Tube Study of the Vibrational Relaxation of Nitric Oxide,” *Journal of Chemical Physics*, Vol. 36, No. 10, 1962, pp. 2597–2603.
<https://doi.org/10.1063/1.1732339>
- [82] Bose, D., and Candler, G. V., “Thermal Rate Constants of the $N_2 + O \rightarrow NO + N$ Reaction Using ab Initio 3A” and 3A’ Potential Energy Surfaces,” *Journal of Chemical Physics*, Vol. 104, No. 8, 1996, pp. 2825–2833.
<https://doi.org/10.1063/1.471106>
- [83] Cruden, B., and Brandis, A., “Measurement and Prediction of Radiative Non-Equilibrium for Air Shocks Between 7–9 km/s,” AIAA Paper 2017-4535, 2017.
<https://doi.org/10.2514/6.2017-4535>

- [84] Streicher, J., Krish, A., and Hanson, R., "Coupled Vibration-Dissociation Time-Histories and Rate Measurements in Shock-Heated, Nondilute O₂ and O₂-Ar Mixtures from 6000 to 14000 K," *Physics of Fluids*, Vol. 33, No. 5, 2021, Paper 056107.
<https://doi.org/10.1063/5.0048059>
- [85] Gimelshein, S., Wysong, I., Bykova, N., Shatalov, O. P., and Zabelinskii, I. E., "Improved Analysis of O₂ Ultraviolet Absorption Spectra Under Nonequilibrium Shock Conditions," *AIAA Journal*, Vol. 58, No. 10, 2020, Paper 058961.
<https://doi.org/10.2514/1.J058961>
- [86] Cruden, B., and Brandis, A., "Updates to Neqair Radiation Solver," NASA ARC-E-DAA-TN19271, NASA, Moffet Field, CA, 2014.
- [87] Ivanov, M., Gimelshein, S., and Kashkovsky, A., *Real Gas Effects on Rarefied Hypersonic Flow over a Concave Body*, Wiley, Hoboken, NJ, 1995, pp. 263–279.
- [88] Varga, Z., Meana-Paneda, R., Song, G., Pauku, Y., and Truhlar, D. G., "Potential Energy Surface of Triplet N₂O₂," *Journal of Chemical Physics*, Vol. 144, No. 2, 2016, Paper 024310.
<https://doi.org/10.1063/1.4939008>